

**Development of hydrophilic polyamide imide microfiltration/ultrafiltration
membranes for oil sands produced water treatment**

by
Nusrat Helali

A thesis submitted in partial fulfillment of the requirements for the degree of
Master of Science

Department of Mechanical Engineering
University of Alberta

© Nusrat Helali, 2020

Abstract

Endless growth of petrochemical, metallurgical, and food industries has resulted in massive water pollution caused by oily materials. Membrane separation processes is one of the fastest emerging technologies for oily wastewater treatment due to their distinct advantages over traditional processes, primarily lower compact design and high product quality. However, fouling of membranes by the adhesion of oil onto the membrane surface and inside its' pores is a major challenge for effective treatment of oily wastewater. We used a novel hydrophilic polymer, polyamide-imide (PAI), to make hydrophilic and underwater superoleophobic microfiltration membranes via non-solvent induced phase separation technique. In the first work, we modified the membranes with hydrophilic additives, including polyethylene glycol (PEG, 0.4 and 6 kDa) and polyvinylpyrrolidone (PVP, 10 and 360 kDa) to improve their hydrophilicity further via blending approach. Oil rejection experiments were conducted to evaluate the reusability of the synthesized membranes. The use of additives resulted in a wide range of membrane morphology, porosity, pore size, and surface chemical property, which affected the permeation rate and flux recovery. However, all synthesized membranes showed >98% rejection of oil. The optimized membranes had underwater superoleophobic property ($\text{OCA} > 150^\circ$) and showed almost 98% pure water flux recovery ratio. This study proposes a facile approach of making superhydrophilic and underwater superoleophobic membranes.

In the second work, we applied a facile layer by layer (LbL) assembly approach for improving the hydrophilicity and selectivity of base PAI membranes using water soluble polyelectrolytes: polydiallyldimethylammonium chloride and polyacrylic acid. The pure water flux declined dramatically with increasing number of coated layers. The antifouling

property of the modified membranes against humic type organic foulants in oil sands produced water was investigated. Pristine PAI membrane showed 62% rejection of organic matters, while the rejection increased up to 65% with the deposition of four bilayers. Simultaneously, the permeate flux decline improved by 26%. All the membranes showed 100% water flux recovery, which shows excellent antifouling property of PAI membranes. This study proposes that due to the presence of inherent hydrophilic functional group on PAI polymer, PAI membranes can be efficiently used as a substrate for LbL deposition. The number of bilayers can be further increased to obtain targeted selectivity and antifouling property.

Preface

This thesis highlights the first applications of PAI polymer for synthesizing porous MF membranes for the treatment of oily wastewater.

Chapter 2 of this thesis “Development of underwater superoleophobic polyamide-imide (PAI) microfiltration membranes for oil/water emulsion separation” has been published in *Separation and Purification Technology* 238 (2020) 116451. doi: 10.1016/j.seppur.2019.116451.

Parts of this work have also been presented in *North American Membrane Society 28th Annual Meeting (NAMS 2019)*, Pittsburgh, PA, USA, May 11-15, 2019, and *11th Western Canadian symposium on water quality research*, Alberta, Canada, May 10, 2019.

Chapter 3 entitled “Layer by layer assembly of polyamide Imide (PAI) membrane by electrostatic deposition of polyelectrolytes for SAGD produced water treatment.” has been prepared for submission. I am the first author of these two works.

Acknowledgement

I expressed my profound gratitude and regards to my supervisor Dr. Mohtada Sadrzadeh. He has been an excellent support and guide throughout my journey. I really grateful to him for giving me an opportunity in his research group to pursue master's degree. He always did counseling during stressful time in the research. His critical review and comments always helped me taking the path of my research in right direction.

I would like to thank my fellow colleagues Amin Karkooti, Laleh Shamaeighahfarokhi, Pooria Karami, Behnam Khorshidi, Simin Shabani, Ali Mohammadtabar, Farshad Mohammadtabar, Hadi Nazaripoor, Nandini Debnath, Muhammad Islam, Asad Asad, Sadaf Naomani, Masoud Rastgar, and Sadegh Aghapour for providing me helpful suggestions, helping in experiments, idea discussion and necessary trainings. I would like to thank my husband Md Farhad Ismail, with whose support and rigorous guidance I could successfully conduct my research.

The thesis is dedicated to my father who left me just five days before joining school, who I couldn't see in his last minutes and my three-year-old son who was genuinely cooperative throughout this journey.

Contents

CHAPTER 1: Introduction	1
1.1 Background and overview	1
1.2 Membrane technology for oily wastewater treatment	4
1.3 Pressure driven membrane processes	5
1.4 Transport phenomena through membranes	6
1.5 Synthesis techniques of membrane	8
1.5.1 Phase inversion technique	9
1.6 Literature review	10
1.6.1 Blending with other hydrophilic polymers and nanoparticles	11
1.6.2 Surface modification	12
1.7 Objectives.....	14
1.8 Thesis Outline.....	15
Chapter 2: Development of underwater superoleophobic polyamide-imide (PAI) microfiltration membranes for oil/water emulsion separation	16
2.1 Introduction	16
2.2 Materials and Methods	18
2.2.1 Chemicals	18
2.2.2 Membrane fabrication	19
2.2.3 Viscosity of casting solution	20
2.3. Membrane characterization	20
2.3.1. Chemical composition tests.....	20
2.3.2. Morphology study	20
2.3.3. Wettability.....	20
2.3.4. Underwater oil wettability.....	20
2.3.5. Surface Roughness	21
2.3.6. Surface energy	21
2.3.7. Hydraulic permeability:.....	22
2.3.8. Porosity.....	23
2.3.9. Average pore size	23
2.3.10 Oil/Water emulsion separation test.....	24
2.3.11 Preparation and characterization of oil/water emulsion	24

2.4. Results and discussions	25
2.4.1. ATR-FTIR results.....	25
2.4.2 Cross-section morphology.....	26
2.4.3. Surface roughness and wettability.....	30
2.4.4. Surface free energy.....	33
2.4.5. Underwater oil wettability.....	34
2.5. Permeation properties of membranes	36
2.5.1. Porosity of membranes.....	36
2.5.2 Compaction factor	37
2.5.3. Hydraulic permeability.....	38
2.5.4. Average pore size of membranes.....	38
2.6. Oil removal experiments	39
2.6.1. Comparison of membranes.....	39
2.6.2. Reusability of membranes	41
2.7. Conclusion.....	44
Chapter 3: Layer by layer assembly of polyamide Imide (PAI) membrane by electrostatic deposition of polyelectrolytes for SAGD produced water treatment.....	46
3.1 Introduction	46
3.2 Materials and Methods	50
3.2.1 Materials	50
3.2.2 Layer by layer membrane modification.....	50
3.2.3 Crossflow membrane filtration setup	50
3.3 Characterization techniques.....	51
3.3.1 Experimental methodology	51
3.3.2 Field emission scanning electron microscope-energy dispersive X-ray (FESEM-EDX)	52
3.3.3 Zeta potential measurement:.....	52
3.3.4 Contact angle.....	52
3.4 Results and discussion.....	53
3.4.1 Surface charge	53
3.4.2 FESEM-EDX.....	55
3.4.3 ATR-FTIR results.....	56
3.4.4 Surface wettability:.....	57

3.4.5 Hydraulic permeability:.....	58
3.4.6 Filtration of BFW	59
3.5 Conclusion.....	62
Chapter 4: Conclusion and future work	63
4.1 Conclusion.....	63
4.2 Future work	65

List of tables

Table 2.1. Chemical structure and other characteristics of PAI.	18
Table 2. 2. Membrane’s preparation variables with corresponding levels (T=293 K and shear rate =50 s ⁻¹).	19
Table 2. 3. Surface characterization parameters of all synthesized membranes.	32
Table 2. 4. Non-polar (LW) and polar components (+, -) of the surface tension, the free energy of cohesion (ΔG_{SLSTOT}).	34
Table 2. 5. Permeation properties (flux and rejection), pore size, and porosity of the synthesized membranes.	36
Table 3. 1. Specification of a typical BFW	47

List of figures

Figure 1. 1. Schematic illustration of SAGD process. Reprinted from [10] with permission from elsevier.....	3
Figure 1. 2. Schematic of membrane classification. Reprinted from [10] with permission Elsevier	6
Figure 1. 3. Fabrication techniques for preparation of the polymeric membranes. Reprinted with permission from [19].	9
Figure 2.1. The size distribution of oil droplets in the feed solution.	25
Figure 2.2. (a) ATR-FTIR spectra of the pristine and modified membrane, (b) FTIR spectra at scanning range of 1460-1800 cm^{-1} , and (c) FTIR spectra at scanning range of 1000-1460 cm^{-1} . ..	26
Figure 2.3. Cross-sectional FESEM images of (a) M1, pristine membrane (b) M2, PAI-PEG 0.4 kDa, (c) M3, PAI-PEG 6 kDa, (d) M4, PAI-PVP 10 kDa, and (e) M5, PAI-PEG 360 kDa.	28
Figure 2.4. AFM 3D images of all synthesized membranes.....	31
Figure 2.5. Digital images of water and oil underwater droplets over surfaces of different fabricated membranes.....	35
Figure 2.6. Variation of flux for different transmembrane pressure at steady state and (b) Trend of flux decline during compaction.	37
Figure 2.7. Permeate flux decline over time due to oil fouling for all synthesized membranes....	41
Figure 2.8. (a) Variation of normalized flux (J_w/J_{w0}), (b) Percentage of flux decline, and (c) Flux recovery ratio at 0.5 bar transmembrane pressure for three consecutive cycles of oil/water emulsion treatment.	43
Figure 2.9. Oil rejection in three consecutive emulsion treatment cycles and optical pictures of feed and permeate solutions.	44
Figure 3.1. Process flow diagram of a typical SAGD process.	47
Figure 3. 2. Schematic of Crossflow filtration set-up. Reprinted with permission from [107].	51
Figure 3.3. (a) Variation of zeta potential due to deposition of PDADMAC and PAA onto membrane surface, (b) Zeta potential of polycation PDADMAC and polyanion PAA.	54
Figure 3. 4. FESEM-EDX of all the membranes before filtration.....	56
Figure 3. 5. ATIR-FTIR spectra of all the membranes for scanning range 1200–2000 cm^{-1}	57
Figure 3. 6. Experimental image of water contact angle for synthesized membranes.	58
Figure 3. 7. Variation of hydraulic permeability of membrane with different number of bilayer deposition.	59

Figure 3. 8. Permeate flux decline over time due to organic fouling for all membranes. 60

Figure 3. 9. (a) Flux decline (FD), organic matter rejection (R) and flux recovery ratio (FRR) of membranes, taken averaged over three samples. In all the cases 100% water flux recovery and almost same rejection performance was observed and (b) Image of BFW and permeate of all membranes..... 62

NOMENCLATURE

Abbreviations

PAI	Polyamide Imide
PVP	Polyvinylpyrrolidone
PEG	Polyethylene glycol
PSf	Polysulfone
PES	Polyethersulfone
OCA	Underwater oil contact angle
WCA	Water contact angle
MWCO	Molecular weight cut-off
RMS	Root mean square
PWF	Pure water flux
FD	Percentage of flux declination
FRR	Flux recovery ratio
LbL	Layer by layer
PDADMAC	Polydiallyldimethylammonium chloride
PAA	Polyacrylic acid
BBD	Boiler Blow Down
DOM	Dissolved Organic Matter
BFW	Boiler Feed Water
MF	Microfiltration
UF	Ultrafiltration
NF	Nanofiltration
RO	Reverse Osmosis
OSPW	Oil Sands Process Affected Water
OTSG	Once Through Steam Generator
SAGD	Steam Assisted Gravity Drainage
TFC	Thin Film Composite
TOC	Total Organic Carbon
TDS	Total dissolved Solids

Symbols

H_p	Pure water permeability ($\text{Lm}^{-2}\text{h}^{-1} \text{bar}^{-1}$)
C	Concentration of solute (mol/L)
dh	Hydraulic diameter (m)
D	Diffusion coefficient (m^2/s)
J	Flux ($\text{Lm}^{-2}\text{h}^{-1}$)
k	Mass transfer coefficient (m/s)
R_m	Intrinsic hydraulic resistance
r_p	Average pore size of membrane (nm)
T	Absolute temperature (K)
V	Variance
v	Cross flow velocity (m/s)
ε	Porosity of membrane support
μ	Dynamic viscosity (m^2/s)
π	Osmotic pressure (bar)
ΔP	Transmembrane pressure (bar)

CHAPTER 1: Introduction

1.1 Background and overview

Freshwater crisis has been drawing the attention worldwide for decades. Nowadays, daily human necessities, industrial growth, agricultural purposes, are escalating this crisis year by year. About 300 million people around the world are living in the places which have water shortage, and this number will grow till 2025 to 1800 million [1]. Poor access to clean and safe drinking water causes several million deaths every year. Seawater comprises 97.5% of the worlds' water resource while the freshwater is only 2.5%, two third of this is frozen in glacier [1]. Exponential growth of industrialization has triggered an increase in the need of freshwater supply and has become a source of existing freshwater pollution. The lack of freshwater now has been calling for numerous efforts toward the improvement of existing water treatment processes and development of new techniques to produce potable water from seawater and to recover usable water from industrial and municipal wastewater streams.

Oil and gas companies generate around fifty-seven barrels of produced water per barrel of oil. This amount adds up to worldwide production of 2.4 billion US gallons of wastewater per day which needs either treated or needs to be properly disposed [2]. In these industries, most of the energy required is either in the form of electrical energy or thermal energy which is produced by burning fossil fuels. On the other hand, almost all kinds of energy production needs water in at least one stage of production. Processes like thermal and nuclear power plants needs an immense amount of water for cooling and fuel processing. In oil and natural gas production industries, water is the most vital commodity for drilling and extraction activities which include oil extraction, processing, waste disposal and land reclamation [3].

Among the numerous contaminants, the oily wastewater originating from oil and gas industry contains oil in the form of emulsion which is hard to remove for recycling or disposal [4,5]. For this purpose, companies usually adopt chemical coagulation, which is a costly method and often remains inefficient for emulsion removal. It requires to use

expensive and hazardous chemicals as coagulant which produce huge amount of sludge which creates additional hassle of disposal. The sludge is disposed, typically by dumping to an off-site reservoir or in an open pit where it adds another associated with the contamination of natural water resources [4]. Canada's oil sands industries are one of the examples who needs innovative and cost-efficient technologies, as well as improvement in existing water management processes since they use massive scale of water for bitumen extraction. *In-situ* methods are the mostly deployed method for oil extraction process since through this method oil can be extracted from deep underground wells. In *in-situ* processes, namely steam assisted gravity drainage (SAGD), steam is injected underground to reduce the viscosity of bitumen. Steam is injected through injection well placed above production well which causes bitumen to melt and flow down in the production well (Fig. 1.1). This liquid bitumen and steam condensate mixture is then pumped out of the production well, where steam condensate is separated from the bitumen and send for being used as boiler feed water (BFW). The water required for carrying out SAGD process is acquired from neighboring rivers and underground water. The SAGD process creates huge amount of wastewater containing organic matters to be disposed, which has drawn negative attention to environmentalists [6]. Current inefficient water treatment techniques in the SAGD operation enhance demands on finite freshwater resources, which push the limits of environmental sustainability. Conventional water treatment methods cannot effectively remove water contaminants, particularly, silica and divalent ions (~85% removal rate) and organic matter (no removal). In addition, water recovery in the current in-situ scheme is 80% [7,8]. The overall average freshwater requirements for the SAGD process is approximately 0.3 barrels of water consumed per barrel of oil produced. Water management, therefore, is critical to oil sands industry, and they are continuously seeking novel technologies for water treatment processes [9]. In addition, to mitigate the environment pollution by waste disposal, oil sands industries are seeking alternative water treatment methods to reduce the usage of freshwater and to recycle water as much as possible.

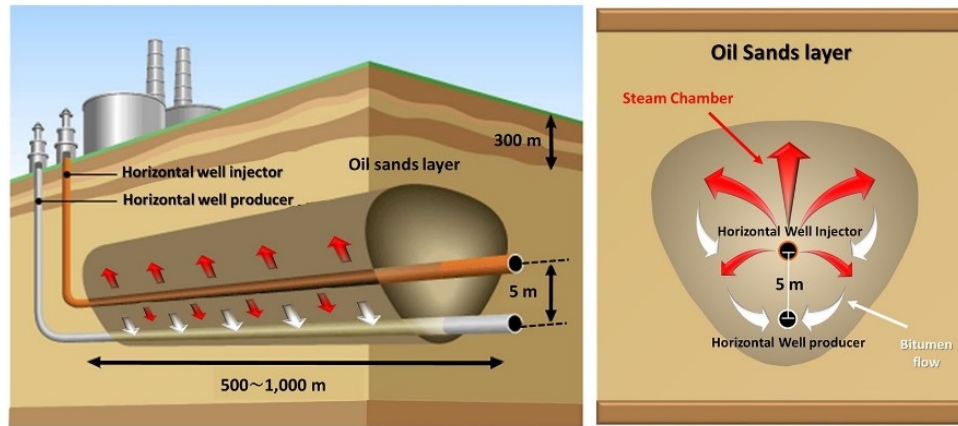


Figure 1. 1. Schematic illustration of SAGD process. Reprinted from [10] with permission from elsevier.

Oil is one of the major pollutants present in the produced wastewater from the oil-gas industries. There are several technologies available for oily wastewaters treatment. The concentration and size of dispersed/emulsified oil in these waters determines which treatment technology should be adopted. Oil/water mixtures can be classified into three broad categories based on oil droplet diameter d : free mixtures $d > 150 \mu\text{m}$, dispersions $20 < d < 150 \mu\text{m}$, and emulsions $d < 20 \mu\text{m}$ [11]. Emulsions can be either oil-in-water (oil as the dispersed phase, water as the continuous phase) or water-in-oil (water as the dispersed phase, oil as the continuous phase) which depends on surfactant type, volumes of both phases, temperature, pH, and other factors [11]. Due to the reasonable efficiency of gravity-based separation technologies for the treatment of free and dispersed oil/water mixtures they are often utilized as the major treatment technique for oily wastewaters. The retentate from these processes usually contain oil in an emulsified form, which remain stabilized by surfactants, polymers, asphaltenes, or other solids which habitat at the oil-water interface [11]. There are several technologies existing for the treatment of the remaining emulsified oil. These technologies include chemical coagulation, dissolved air filtration, hydrocyclones, media filtration, and polymeric or ceramic membranes. The treatment process to be adopted is determined based on power requirements, footprint and weight, oil and other particulate rejection, and cost [6,11,12]. In this thesis, we focus on the treatment of produced wastewater generated from oil and gas industries by membranes.

1.2 Membrane technology for oily wastewater treatment

Polymeric/ceramic microfiltration (MF) and ultrafiltration (UF) treatment processes are promising to the treatment of oily wastewater and are able to constantly treat oil in water emulsions, which also contain other suspended solids. MF and UF use less energy compared to other technologies and are highly modular and simple processes [2]. Due to these advantages, MF and UF treatment technologies have become the most preferred approach for oily wastewater treatment [4,11].

In addition to the removal of emulsified oil from water, many produced water streams also require desalination for reclamation or reuse. For desalination purpose, thermal technologies are frequently utilized although reverse osmosis (RO) based technologies would outperform them and may eventually be adopted for these highly salty feed waters treatment [13]. Hence, membrane-based technologies have potential for replacing previously established technologies for oily wastewater treatment and for desalination as well. One of the main obstacles behind using RO for the desalination of oil sands produced water is that RO membranes have an extremely low tolerance for oil along with other foulant in the feed stream [14]. Oil and grease fouling can cause irreversible and severe decline in permeability and may cause permanent degradation of the membrane. Particularly, organic emulsions, can form a deposited film on the membrane surface, which needs to be removed before membrane filtration. A renowned manufacturer of RO membranes, Dow Filmtec, recommends the concentration of oil in membrane feed stream to be as low as 0.1 mg/L. Given that, oily wastewater must be pre-treated before being housed to an RO process, it must be noted that , if desalination is the ultimate target of wastewater treatment, a hybrid process which includes pretreatment of produced wastewater for organic foulant removal followed by employing RO and nanofiltration (NF) would be more efficient rather than a single step RO and NF [11].

As the size of oil droplet in a typical oily wastewater ranges from 1 to 10 μm , UF and tighter MF membranes are the more relevant treatment choices. Although, MF and UF membranes can be severely affected by free, dispersed, and emulsified oil fouling [11,15]. Cumulative accumulation of the feed constituents like oil along with other organic matter on the surface of the membrane and inside the pores results in a severe decline in the

permeate flux and affects the permeate water quality. Thus, academia has showed great interest in improving the fouling resistance of membranes. The findings from literature have shown that by increasing the hydrophilicity of membrane the anti-fouling property of a membranes can be increased [16].

1.3 Pressure driven membrane processes

Membranes are classified in terms of the size of solutes they reject. Membranes are classified into four broad categories; MF, UF, NF and RO. The pore size of MF membranes ranges from 0.01 to 10 μm and are able to retain macromolecules, suspended solids, virus and bacteria. The pore size of UF membranes ranges from 10 to 100 nm, which is able to retain bacteria, viruses, and macromolecules such as proteins ($M_w > 10$ kDa). NF membranes have pore sizes between 1 to 10 nm and are mainly used for separating divalent ions. The pore size of RO membranes is less than 1 nm [17]. RO membranes are used for rejecting salts and thus are used for desalinating sea and brackish water (Fig. 1.2).

Based on internal structures, membranes can be categorized as symmetrical or asymmetrical. The symmetrical membranes have uniform pore sizes throughout the cross-section. On the other hand, asymmetric membranes have smaller pores close to the top surface and larger pores far away from top surface [17]. There exists a dense skin layer on the top of the membrane with the thickness around 500 nm or above and a porous sublayer exist beneath the skin layer with thickness up to 200 μm . The skin layer controls the retention and transport of solutes while the sublayer provides mechanical strength against high operating pressure [17].

Often asymmetric membranes provide higher permeation rate compared to symmetric membrane of same thickness [17]. Generally, permeation rate is inversely proportional to membrane thickness. A membrane which provides desired retention of solute with a high permeation rate is always desirable, thus a thin membrane with high product quality is considered an ideal membrane [17].

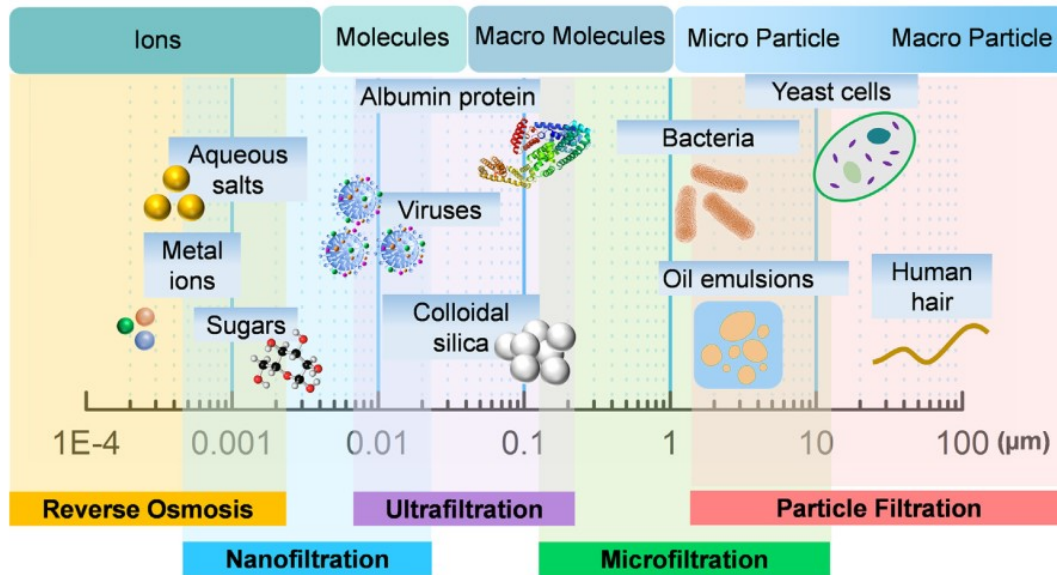


Figure 1. 2. Schematic of membrane classification. Reprinted from [10] with permission Elsevier. Based on pore volume, membranes can be classified as dense or porous membrane. In NF and RO membranes, molecule transportation occurs based on solution-diffusion mechanism [18]. The molecules of solute and solvent which are transferring through the membrane, are first dissolved in the membrane, then diffuse through the membrane, and finally desorbed at the permeate side. Owing to difference in solubility and diffusivity of the components within the membranes, separation in NF/RO membranes takes place. In the case of porous MF and UF membranes, the transport mechanism is based on pressure-driven convection through the pores. The mechanism responsible for separation of component in these porous membranes is known as molecular sieve mechanism i.e.; retention of solutes based on particle size.

1.4 Transport phenomena through membranes

The resistance for water passage through a membranes consists of three major components, namely , 1) the hydrodynamic resistance of the membrane in the absence of foulants, 2) the resistance due to the accumulation of ions at the membrane surface (concentration polarization), and 3) the resistance due to the accumulation of fouling materials at the membrane surface (cake layer formation). The hydrodynamic resistance of the membrane itself in the absence of foulants is calculated by measuring pure water flux at different

transmembrane pressure (J_0 , m³/m²s). Membrane resistance (R_m , 1/m) is then calculated using Darcy's law as follows [17]:

$$J_0 = \frac{\Delta P}{\mu R_m} \quad (1.1)$$

where J_0 is the pure water flux across membrane, ΔP is transmembrane pressure, and μ is viscosity of the permeate. The hydraulic resistance of porous MF/UF membranes can be calculated using Hagen-Poiseuille equation:

$$R_m = \frac{8\delta_m}{n_p \pi r_p^4} \quad (1.2)$$

where δ_m is the thickness of membranes, n_p is the number of pores per unit membrane area, and r is the pore radius. According to Eqn. 1.1 and 1.2, the transport through the membranes is directly proportional to the fourth power of pore radius. The resistance due to the accumulation of foulants at the membrane surface (concentration polarization) is measured by generated transmembrane osmotic pressure ($\Delta\pi$). $\Delta\pi$ reduces the effective pressure for water transport and the Darcy's law can be written as follows:

$$J = \frac{\Delta P_t - \Delta\pi}{\mu R_t} \quad (1.3)$$

Where J is the permeate flux, and R_t is the total resistance against mass transfer. In the case of transport through MF/UF membrane, the osmotic pressure is often neglected since the main contribution to osmotic pressure is generated from the low molecular weight solute passing through the membrane [17].

R_t , total resistance in Eqn 3, which can be described as follows:

$$R_t = R_m + R_c + R_{cp} + \dots \quad (1.4)$$

where R_c is the resistance of formed cake layer on membrane surface, and R_{cp} is the resistance due to build-up of concentration polarization.

At steady-state conditions, the equation relating concentration polarization and flux, and mass transfer coefficient, can be expressed as:

$$\frac{C_m - C_p}{C_b - C_p} = \exp\left(\frac{J\delta}{D}\right) \quad (1.5)$$

where C_m , C_p , and C_b are concentrations of solute on the membrane surface, in permeate, and in feed bulk respectively. The ratio of the diffusion coefficient and the thickness of the boundary layer (δ/D) is called the mass transfer coefficient k . The intrinsic (real) rejection of a membrane is calculated using the following equation:

$$R = 1 - \frac{C_p}{C_m} \quad (1.6)$$

Combining Eqn. 5 and 6 gives:

$$\frac{C_p}{C_m} = \frac{\exp\left(\frac{J}{k}\right)}{R + (1 - R)\exp\left(\frac{J}{k}\right)} \quad (1.7)$$

The $\frac{C_p}{C_m}$ is called the concentration polarization modulus and is a semi-quantitative measure of the extent of concentration polarization [17]. A higher concentration polarization modulus value suggests a high tendency for occurrence of concentration polarization.

1.5 Synthesis techniques of membrane

There exist several methods to synthesize dense and porous membranes. Some common methods are sintering, stretching, track-etching, phase inversion, interfacial polymerization, and solution casting as presented in Fig. 1.3 [17]. The selection of any method depends on the desired properties of the targeted membrane. Phase inversion is the most common method for fabricating porous membranes.

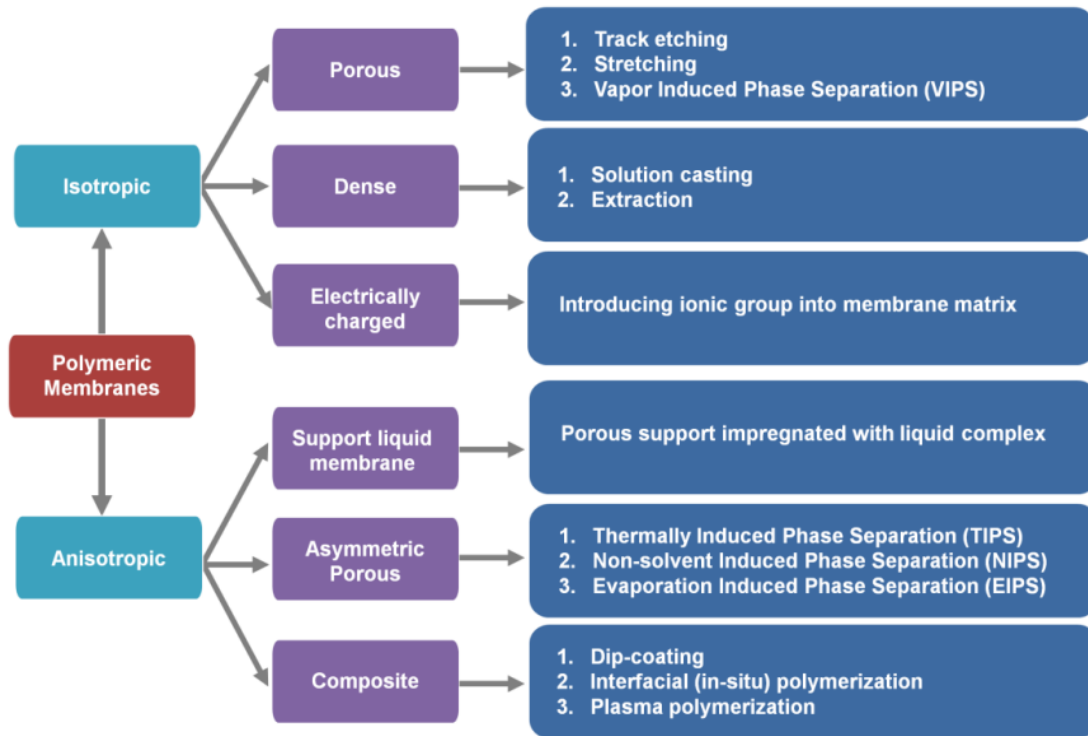


Figure 1. 3. Fabrication techniques for preparation of the polymeric membranes. Reprinted with permission from [19].

1.5.1 Phase inversion technique

Phase inversion is the most versatile method for preparing porous polymeric membranes. During the phase inversion, when a thermodynamically stable polymer solution is immersed in non-solvent, phase separation occurs and leaves a polymer rich porous film and a polymer lean phase [20].

Available techniques for phase inversion are [20]:

1. Immersion precipitation (NIPS): induced by immersion of polymer film into nonsolvent bath.
2. Precipitation by evaporation (EIPS): induced by evaporating the volatile solvent from polymer that was dissolved in solvent mixture.
3. Thermal precipitation (TIPS): induced by lowering the temperature below a certain degree.

4. Precipitation from vapor phase (VIPS): induced by immersing polymer film in a nonsolvent vapor phase.

Among the above-mentioned methods, immersion precipitation technique, NIPS method, is utilized in this study. In this technique, a polymer solution is cast as a thin layer on flat glass and immersed into a nonsolvent bath which is mainly water. Upon immersing in water, solvent diffuses into nonsolvent phase due to high miscibility of solvent into nonsolvent. After some time, the composition of the polymer rich phase reaches the glass transition composition and the system solidifies.

In immersion- precipitation, the structure can be changed from porous to nonporous and vice versa by varying the following parameters [17]:

- i. Polymer type (charge density, molecular weight, and crystallinity)
- ii. Solvent- nonsolvent pair
- iii. Concentration and viscosity of polymer solution
- iv. Temperature and composition of polymer solution and coagulation bath
- v. Location of liquid-liquid de-mixing gap (position of binodal curve in ternary diagram)

In immersion- precipitation, the role of rate of exchange between solvent and nonsolvent is critical in the final membrane structure. The exchange rate can be modified by altering the composition of polymer solution and coagulation bath [21].

1.6 Literature review

The asymmetric porous MF/UF membranes are generally synthesized by phase inversion process where, a polymer solution is cast onto a suitable support by using a film applicator, and then immersed into a coagulation bath. Fouling reduces the life of a membrane and is a major challenge affecting the sustainability of membrane-based treatment processes. High susceptibility of porous membranes to pore blocking by foulant results in an irreversible fouling, which results in a remarkable loss in permeation rate [5]. It is well established that by improving hydrophilic additives, the adhesion of organic foulants on the membrane surface could be reduced, which consequently, lessens membrane fouling and improves permeate water quality [22]. To date, numerous approaches have been

proposed to improve the antifouling property of membranes either by blending the base polymer with hydrophilic additives, hydrophilic nanoparticles or altering the surface hydrophilic properties via chemical or physical modification.

1.6.1 Blending with other hydrophilic polymers and nanoparticles

The approach of blending the main polymer with polymeric additives has been exclusively utilized for improving final membrane properties as it provides a facile preparation technique. Blending provides a wide range of versatility in incorporating targeted properties on the membrane [22]. Hydrophilic additives such as hydrophilic polymers, amphiphilic copolymers and inorganic nanoparticles have been introduced in order to enhance permeation rate and antifouling property in numerous studies [23]. Polyvinylpyrrolidone (PVP) and polyethylene glycol (PEG) are two most common additives used for polymeric blending which increased the hydrophilicity and permeability of asymmetric membrane [23]. Ochoa et al. blended a hydrophilic poly (methyl methacrylate) (PMMA) additive with hydrophobic polymer, polyvinylidene fluoride (PVDF) to synthesize PVDF UF membrane [5]. The hydrophilicity and surface porosity of the synthesized PVDF membranes were found to enhance upon increasing PMMA loadings which consecutively enhanced water permeability. The membranes which had highest loading of PMMA could also reduce the deposition of foulants on the membrane surface [5].

Incorporation of inorganic nanoparticles into the porous membranes has also been widely investigated for improving hydrophilicity and porosity of porous membranes [24]. Most of the previous studies have integrated single-element nanoparticles, e.g., Al_2O_3 , Fe_3O_4 , TiO_2 and SiO_2 , into the porous membranes [25]. Yan et al. reported significant improvement in antifouling and permeation properties of PVDF membranes by incorporating Al_2O_3 nanoparticle [26]. Ghaemi and coworkers blended surface modified Fe_3O_4 nanoparticles with polyethersulfone (PES) polymer and found an increase in hydrophilicity and permeation properties [27]. Khorshidi et al. incorporated indium tin oxide (ITO) in PES to synthesize mix matrix nanocomposite membranes for the treatment of oil sand produced

water. The organic matter rejection percentage of the PES/ITO nanocomposite membrane was found to be higher than pure PES membrane. The thermal resistance and electric conductivity of the nanocomposite membrane was also improved [28].

Recently, the incorporation of carbon-based nanomaterials into porous membranes has been widely studied. Vatanpour et al. incorporated multiwalled carbon nanotubes (MWCNTs) coated by titanium dioxide (TiO₂) nanoparticles into PES membranes for oily wastewater treatment [29]. It was found that 0.1 wt. % of TiO₂ coated MWCNT membrane showed the best antifouling property due to its synergistic photocatalytic activity. Wang et al. prepared GO blended PVDF nanocomposite UF membrane. Incorporation of GO improved the hydrophilicity and increased pure water flux recovery [30].

Although blending method was found to be effective in enhancing the hydrophilicity to the main polymer, the major challenge regarding the leaching of additives during crossflow filtration have restricted the practicality of this approach. For example, PEG and PVP are dissolvable in water and the membrane might lose its initial structure, surface properties (hydrophilicity, charge and roughness), and thermomechanical properties over time. In the case of incorporating nanomaterials to the polymer, a poor adhesion between nanomaterials and the polymeric material will lead to the leaching of these materials out of nanocomposite membranes, resulting in a steady destruction of the membrane over time, decreasing performance robustness and potentially causing many environmental issues [31].

1.6.2 Surface modification

The surface modification of a porous membrane involves the binding of some additional properties (affinity, responsiveness or catalytic) to enhance the performance of the membrane. The surface modification focuses on, i) minimizing fouling by increasing the repulsion between membrane surface and/or pores and foulant on the feed, ii) increasing the selectivity towards a foulant or even entirely altering separation functions [32]. Ion beam irradiation, plasma irradiation and vapor phase deposition, grafting, coating and acid base treatment are some of the physical and chemical surface modification technique [33].

Surface-coating involves depositing a thin layer of coating material directly on the top of a membrane surface. By surface-coating, NF membrane could be prepared using porous

UF/MF membranes as a substrate. Ma et al. coated poly (vinyl alcohol) (PVA) onto the surface of PES membrane, followed by crosslinking of PVA to enhance the antifouling property [34]. The hydrophilicity increased due to deposition of PVA chains over the surface of membrane while the coating declined the water flux substantially. A novel composite membrane was prepared by LbL assembly of chitosan (CHi)/polystyrene sulfonate (PSS) polyelectrolyte on PES membrane [35]. The filtration performance of membrane with 9-bilayer CHi/PSS showed 95% rejection of BSA. Layer-by-layer deposition of anionic and cationic polyelectrolytes can readily transform porous MF/UF membranes into NF membrane. Malaisamy et al. deposited PSS/protonated poly(allylamine) (PAH) and PSS/ polydiallyldimethylammonium chloride (PDADMAC) onto PES UF membrane via LbL-assembly [34]. The MWCO of the main membrane reduced significantly. The selectivity of chloride/sulfate for the PSS/PDADMAC coated PES membrane was increased.

This surface modification techniques, such as plasma treatment, UV treatment, chemical grafting, chemical vapor deposition (CVD), plasma CVD, and LbL assembly have been found very effective in fouling reduction [36]. The main challenges of the first five techniques are the high cost of surface modification and difficulty in scaling up the modification process for a large membrane surface area. On the other hand, LbL assembly is more flexible and straightforward, and it is also applicable to create ultrathin films of larger surface area from various materials. However, there are still challenges regarding the attachment of layers on the membrane surface. Since, the first layer is the most important one, the presence of suitable functional groups on the membrane surface becomes critical on the robustness of LBL assembly-modified membranes. The PAI substrate utilized in the present research is negatively charged in all pH values and possess various chemical groups (N-H, C=O, and C-O) in its structure, which makes the attachment of different materials on the surface easier and stronger.

1.7 Objectives

In this thesis, we contribute to the field of oil and gas industries produced wastewater treatment by development of new types of MF/UF membranes. Conventional MF/UF membranes are prepared with polysulfone (PSF) and PES. These membranes suffer from severe fouling due to their hydrophobic nature. These membranes are then further modified for improving the hydrophilicity and antifouling property by complicated physical and chemical modification methods. This provided inspiration to explore new and novel material for synthesizing superhydrophilic porous MF/UF membranes. PAI, a copolymer of amide and imides, commercially known as Torlon®, possess the unique characteristic properties of both polyamide and polyimide. The exceptional mechanical, thermal, and chemical resistant properties as well as superior hydrophilicity, originating from amide and imide functionals make PAI an outstanding candidate for a wide range of membrane application.

The main goal of the research is to synthesize porous MF and UF membranes with a novel hydrophilic polymer PAI by phase inversion technique. The improvement of selectivity and antifouling property was further investigated by modifying the membranes. To achieve this goal, the current work is focused on the following themes:

- (i) Investigating the performance of PAI MF membranes for oily wastewater treatment. The polymer solution was blended with hydrophilic additives such as PVP and PEG to improve membrane permeation properties and oleophobicity. The findings from this study provides a baseline for further integration of hydrophilic (molecular weight, concentration) additives to obtain desired membrane characteristics.
- (ii) Investigating the performance of PAI MF membranes for SAGD produced water treatment. LbL deposition of oppositely charged electrolytes was adopted for improving the surface hydrophilicity for improving DOM selectivity and antifouling properties. The findings from this study provides a guideline for incorporating the required number of polyelectrolyte layers for obtaining desired selectivity and antifouling property.

1.8 Thesis Outline

Chapter 1 of the thesis provides a brief explanation of the SAGD process and the conventional produced water treatment technology used by the oil sands industries. The advantages of membrane-based separation processes over the shortcomings of the existing water treatment technology are discussed. A literature review on application of MF/UF membranes for treatment of oilfield produced water has been presented.

In chapter 2, a superhydrophilic and underwater oleophobic PAI MF membrane was developed and the antifouling property was investigated using a surfactant-stabilized oil/water emulsion. The membranes were further modified by incorporating hydrophilic additives to onto host membrane and the enhancement in anti-oil fouling property was systematically assessed.

In chapter 3, the applicability of PAI membranes to treat the SAGD produced was studied. The advantage of inherent superhydrophilic property of PAI was investigated using BFW. The inherent negative charge density of the polymer was utilized as PAI to be used as a substrate for LbL assembly approach. The number of bilayers were increased, and the organic rejection of BFW and antifouling property was investigated.

In chapter 4, a summary of the major findings from the studies was provided along with a concluding discussion. Moreover, ideas and proposals for further advancement of the current study was provided.

Chapter 2: Development of underwater superoleophobic polyamide-imide (PAI) microfiltration membranes for oil/water emulsion separation

2.1 Introduction

Oil in oily wastewater exists in two main forms: free-floating oil and dispersed or stable emulsified oil [11]. Among the forms of oils existing in oily wastewater, emulsified oil in water has the smallest average droplet size among others ($<20\ \mu\text{m}$). Previous investigations illustrated that emulsified oil can exist in aquatic environments for a prolonged time and thus brings about numerous negative impacts on human health and the surrounding ecosystems [37]. Free-floating oil can be easily separated using conventional gravity separation, but emulsified oil droplets take a very long time for separating from water, which makes this process impractical. To date, many research and development have been undertaken to develop advanced methods to address this issue [38].

Some of the conventional methods based on physical separation for treating oil-contaminated water are adsorption [39,40], water evaporation [41], and membrane-based filtration [42]. Some of the promising approaches based on chemical treatment are electroflotation [43], photocatalysis [44], and ozone treatment [45] have been successfully applied for the purification of oil-contaminated water. To fairly compare the mentioned methodologies, cost, process time, required space for installation, use of toxic chemicals, and possibility in production of secondary pollutants should be considered. Owing to low energy demand and cost efficiency, membrane-based technologies have recently received a huge surge of interest [46]. Membrane processes, particularly microfiltration (MF) and ultrafiltration (UF), can overcome the main disadvantages of traditional techniques, including high operating costs and large environmental footprint. However, the high vulnerability of MF and UF membranes to fouling by oil has limited the advancement of membrane processes for oil/water separation. The adsorption of oil onto the membrane surface and/or within its pores reduces the membrane lifetime and thus increases operating costs of treatment. Hence, many studies have been conducted on the development of new membrane materials with functional properties that reduce the adhesion of oily contaminants to the membrane surface [47–51].

Depending on the affinity of a membrane surface towards water or any non-polar oil, either hydrophilic (or oleophobic) or hydrophobic (or oleophilic) membranes (respective water contact angle (WCA) and oil contact angle (OCA) between $0^\circ \leq \theta \leq 90^\circ$) are chosen for oil/water or water/oil emulsion separation. [52,53]. Because of the intrinsic oleophilicity of hydrophobic materials (also called oil-removing materials), they are easily fouled by oil, making them ill-suited for the treatment of oil-in-water emulsions [54,55]. Hydrophilic materials, on the other hand, are fouling-resistant and show excellent performance in terms of water flux, oil rejection, and reusability upon washing or chemical cleaning. Inspired by the wetting behavior of fish scales, researchers have recently focused on the construction of superhydrophilic and underwater superoleophobic surfaces with OCA more 150° [50,51,56]. Since finding a material that possesses surface energy higher than water and lower than oil is challenging, these types of membranes are primarily developed through grafting new functionalities to a base polymer surface. The incorporated hydrophilic groups increase surface hydrophilicity, and most of the cases increase the surface roughness at the same time. Hence, these membranes are able to absorb abundant water into their micro-/nano-scaled features, which repels oil effectively under water [37,57–61]. However, superhydrophilic and underwater superoleophobic membranes suffer from complex membrane fabrication procedure, upscaling difficulty of developing robust membranes, leaching of grafted materials to feed solution during long-term filtration, and environmental concerns due to the use of toxic reagents for chemical grafting.

In this study, we proposed an easily implemented approach, based on well-established phase inversion method, to synthesize polyamide-imide (PAI) superoleophobic membranes. Conventional MF/UF membranes prepared with polysulfone (PSF) and polyethersulfone (PES) are widely used for oil/water separation [62–64]. These polymers are also used as a primary platform for the development of above mentioned superhydrophilic and underwater superoleophobic membranes. Apart from being inefficient for oil separation (oil rejection much less than 99%), these membranes suffer from severe oil fouling due to their hydrophobic nature. As a result, they require to be regenerated more frequently during operation, which makes the process cost- and energy-intensive in large-scale processes. The exceptional mechanical, thermal, and chemical resistant properties as well as superior hydrophilicity, originating from amide and imide

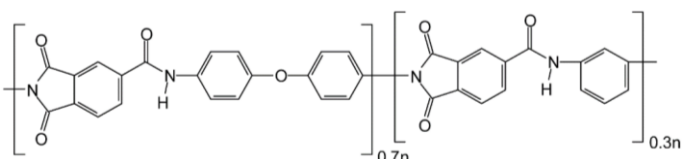
functionals make PAI an outstanding candidate for a wide range of membrane application [65]. Herein, we systematically assessed the overall performance of synthesized PAI membranes for oil/water separation application. Two different kinds of additives, polyvinylpyrrolidone (PVP) and polyethylene glycol (PEG) were used to modify membrane pore structure and improve selectivity as well as anti-fouling properties.

2.2 Materials and Methods

2.2.1 Chemicals

Commercial PAI (Torlon® 4000T-HV, Solvay Advanced Polymers) was used for preparing porous MF membranes. The chemical structure and other properties of PAI are summarized in Table 2.1. Polyvinylpyrrolidone (PVP, reagent grade MW = 10 and 360 kDa) and poly (ethylene glycol) (PEG, reagent grade MW = 0.4 and 6 kDa), supplied by Sigma-Aldrich, were used as polymeric additives. Dimethylacetamide (DMAc, >99.9%, Fisher Scientific) was used as a solvent. To prepare oil in water emulsions hexadecane (> 99%, Sigma-Aldrich) was dispersed in demineralized water, using Tween 80 (Sigma-Aldrich) as a surfactant. Dextran (Alfa Aesar) with different molecular weights (MW=150, 250, and 500 kDa) was used for determining the molecular weight cut-off (MWCO) of the synthesized membranes.

Table 2.1. Chemical structure and other characteristics of PAI.

Name	Polyamide-imide
Commercial name	Torlon® 4000T-HV
Chemical structure	 <p>The chemical structure shows a repeating unit of a polyamide-imide. It consists of two imide rings connected by a central ether linkage (-O-). The first imide ring is part of a 5-membered ring system fused to a benzene ring. The second imide ring is also part of a 5-membered ring system fused to a benzene ring. The two benzene rings are connected at their para positions by an oxygen atom. The repeating unit is shown with brackets and subscripts 0.7n and 0.3n.</p>
Particle size	<150 μm
Viscosity	Highly viscous
Glass transition temperature (T _g)	275 °C

2.2.2 Membrane fabrication

Membranes were fabricated via NIPS method. The phase separation takes place by the diffusion of solvent from polymer solution into non-solvent, followed by solidification of polymer into a coagulation bath. Altogether five polymer solutions were prepared by mixing PAI/DMAc/additives, as shown in Table 2.2. The mixtures were stirred at 40°C for 24 h with a rate of 90 rpm. In the case of PEG 6 kDa, the additive was heated at 60°C for 40 min to improve its solubility in the solvent prior to mixing with the polymer. The polymer-additive mixtures were kept in room temperature for 24 h so that the air bubbles could be removed. To prepare the membranes, polymer solutions were cast on a piece of non-woven polyester fabric with the aid of an automatic film applicator (TQC, Gardco). The gap height between the applicator and the base plate was adjusted to 190 μm , and the casting speed was 5 mm/s. Finally, the cast films were immersed in a coagulation bath containing demineralized water, where an exchange between solvent and non-solvent (water) occurred, and a solidified porous membrane formed. The synthesized membranes were kept in the coagulation bath for two hours to completely leach solvent out of the polymer matrix. Later, the membranes were transferred into another demineralized water bath and kept there until testing.

Table 2. 2. Membrane's preparation variables with corresponding levels (T=293 K and shear rate =50 s⁻¹)

Membrane	PAI (wt%)	Additive (wt%)				DMAc (wt%)	Viscosity of casting solution (cp)
		PEG-400	PEG-6000	PVP-10000	PVP-360000		
M1	12	-	-	-	-	88	1725
M2	12	2	-	-	-	86	1750
M3	12	-	2	-	-	86	1800
M4	12	-	-	2	-	86	1825
M5	12	-	-	-	2	86	6775

2.2.3 Viscosity of casting solution

The viscosity of the polymer solutions was measured with a rotational rheometer (Brookfield DV-III Ultra). The temperature of the apparatus was adjusted at 298 K by a circulating water system. The polymer solution was placed in the cylinder, and the machine measured the shear stress of the solution against rotation.

2.3. Membrane characterization

2.3.1. Chemical composition tests

Chemical composition of the synthesized membranes was evaluated via attenuated total reflection Fourier transform infrared spectroscopy (ATR-FTIR, Bruker, Equinox 55). The ATR-FTIR data were collected at scanning range of 650–4500 cm^{-1} in ambient temperature with a resolution of 4.0 cm^{-1} .

2.3.2. Morphology study

To investigate the effects of additives on membranes structure, the morphology of the fabricated membranes was characterized using a field emission scanning electron microscopy (FESEM). The dried membranes samples were cracked under liquid nitrogen, and the membrane layer was peeled off from polyester fabric support. Cross-sectional images of the membranes were taken using a FESEM instrument (JEOL 6301 F) at two different magnifications.

2.3.3. Wettability

To study the wetting behavior of the synthesized membranes, contact angle between water droplet and the membrane surface was measured by sessile drop method using a contact angle measuring device (Kruss GmbH, Hamburg, Germany). 2 μl of water droplet was placed on the membrane surface by a syringe and contact angle was measured after the droplet reached equilibrium. Five contact angle data were taken for each sample, and the average values were reported.

2.3.4. Underwater oil wettability

The oleophobic behavior of membranes was evaluated by conducting underwater oil contact angle measurement. The oil (hexadecane) contact angle was captured by the captive

bubble technique. Wet pieces of membranes were attached to a glass slide and were submerged in an optically sensitive quartz cuvette filled with demineralized water. Underwater measurement required J-shaped inverted needle to place below the slide with the needle tip facing the membrane surface. 3 μ l hexadecane was placed on the membrane surface, and the measurement was taken when the oil droplet successfully sat on the membrane surface. The contact angle was measured at three different places on the membrane surface, and the average values were reported.

2.3.5. Surface Roughness

The surface topography of the synthesized membranes was investigated using atomic force microscopy (AFM, Bruker Dimension Icon, USA). Area of 10 μ m \times 10 μ m of each membrane was scanned at three different places of the surface with a scanning rate of 5.0 Hz using tapping-mode, and the average surface roughness values were reported.

2.3.6. Surface energy

Surface energy of the membrane was evaluated by extended Young–Dupré and van Oss equation [66]. Lifshitz–van der Waals (LW), negative (–), and positive (+) surface tension components of the solid surface were calculated using this equation. For this experiment, the contact angles of three probe liquids with known values of LW, –, and + surface tension parameters were measured [66,67]. The measured contact angles were plugged in Eqn.2.1 to calculate the non-polar (Lifshitz–van der Waals), negative (–) and positive (+) surface tension components of the solid surface [66,67].

$$\gamma_L^{TOT} \left(1 + \frac{\cos \theta}{r} \right) = 2 \left(\sqrt{\gamma_L^{LW} \gamma_S^{LW}} + \sqrt{\gamma_L^+ \gamma_S^-} + \sqrt{\gamma_L^- \gamma_S^+} \right) \quad (2.1)$$

where θ is the contact angle and the subscripts S, and L correspond to the solid surface (membrane) and liquid, respectively. Superscripts LW, –, and + denote non-polar, electron donor, and electron acceptor components of surface energy, respectively. r in Eqn. 2.1 is the Wenzel roughness factor, which indicates the ratio of actual surface area to the planar area. This factor is calculated as follows [68]:

$$r = 1 + SAD \quad (2.2)$$

where SAD is the surface area difference, representing the percentage of the surface area increased due to roughness. SAD values were derived from AFM results.

According to van Oss theory, the total surface tension (γ^{TOT}) is the sum of nonpolar (Lifshitz-van der Waals, γ^{LW}) and polar (acid-base, γ^{AB}) components [69]. The polar (AB) component of the surface tension comprises electron donor (-) and electron acceptor (+) components, which is calculated using the following equation [66,67],

$$\gamma_s^{AB} = 2 \left(\sqrt{\gamma_s^+ \gamma_s^-} \right) \quad (2.3)$$

The non-polar (LW) and polar (AB) surface tension components are used to calculate the total free energy of cohesion (ΔG_{SLS}^{TOT}) of surface S in Liquid L (water in this case) using Eqn. 2.4 [66,67].

$$\Delta G_{SLS}^{TOT} = -2 \left(\sqrt{\gamma_S^{LW}} - \sqrt{\gamma_L^{LW}} \right)^2 - 4 \left(\sqrt{\gamma_S^+ \gamma_S^-} + \sqrt{\gamma_L^+ \gamma_L^-} - \sqrt{\gamma_S^+ \gamma_L^-} - \sqrt{\gamma_S^- \gamma_L^+} \right) \quad (2.4)$$

Here, water and formamide were selected as the polar liquids, and diiodomethane was selected as the non-polar liquid. The non-polar liquid is used to calculate the non-polar surface tension component [66,67]. Furthermore, high-energy (polar and non-polar) liquids were selected to produce larger and easily measurable contact angles.

2.3.7. Hydraulic permeability:

A dead end stirred filtration cell (Amicon, UFSC40001) with 400 ml solution capacity and effective membrane area of 41.8 cm² was used to conduct hydraulic permeability tests. The filtration cell was connected to a pressurized nitrogen gas line from the top part. Permeate was collected in a beaker and was weighed using a digital balance (ME4002, Mettler Toledo, USA). The weight of permeate was recorded on a computer in every 30 s interval. The pure water flux (PWF) was calculated as follows:

$$J_w = \frac{\Delta Q}{A \rho \Delta t} \quad (2.5)$$

where J_w is the pure water permeation flux ($\text{Lm}^{-2}\text{h}^{-1}$), ΔQ is the permeate volume (L), ρ is the density of permeate at room temperature, A is the effective membrane area (m^2), and Δt is the sampling time (h).

2.3.8. Porosity

The porosity of the membranes was evaluated using the gravimetric method [70,71],

$$\varepsilon = \frac{m_1 - m_2}{\rho_{\text{water}}} \bigg/ \left(\frac{m_1 - m_2}{\rho_{\text{water}}} + \frac{m_2}{\rho_{\text{PAI}}} \right) \quad (2.6)$$

where m_1 and m_2 are the weights of wet and dry membrane samples, respectively. ρ_{water} is the density of water and ρ_{PAI} is the density of PAI polymer at ambient temperature.

2.3.9. Average pore size

The average pore size of the membranes was measured by MWCO method. MWCO refers to the molecular weight (MW) of a specific solute of which the membrane has 90% rejection [72]. The MWCO can be evaluated by conducting rejection test using dilute solutions of charge neutral solutes such as PEG, alkanes, dextran, pesticides, and acids [72,73]. In this study, MWCO measurements were conducted using dextran (MW range of 150-500 kDa), which is easily soluble in water. Solutions (250 mg/L) of three different MWs of dextran were prepared using demineralized water. Before conducting MWCO measurement, membranes were compacted at 1.4 bar to reach a steady PWF. The MWCO measurements were conducted at 0.48 bar. The concentrations of both feed and permeate were examined by a TOC analyzer (TOC-L CPH, Shimadzu, Japan). The rejection of dextran was calculated using the equation below:

$$R_D = \frac{C_F - C_P}{C_F} \times 100\% \quad (2.7)$$

where C_F and C_P are the concentrations of feed and permeate, respectively. The average pore size (r_p , nm) of the membranes was calculated by converting MWCO into pore radius using the following equation [74–76]:

$$r_p = 0.33(\text{MWCO})^{0.46} \quad (2.8)$$

2.3.10 Oil/Water emulsion separation test

To investigate oil/water separation efficiency, and the oil-fouling tendency of the synthesized membranes, the above-mentioned dead-end cell was again used with stirring as following procedure:(1) Compacting the membranes at 1.4 bar to reach a steady PWF, (2) measuring the PWF (J_{w0}) at 0.48 bar, (3) measuring the permeate flux during filtration of oil/water emulsion (J_w), (4) washing the fouled membranes with mild soapy water for 20 seconds followed by splashing of water, and (5) measuring the PWF of washed membranes (J_{w1}) again. The percentage of flux decline (FD) was calculated as follows:

$$FD = \left(1 - \frac{J_w}{J_{w0}}\right) \times 100 \% \quad (2.9)$$

The flux recovery ratio (FRR) was calculated using the following equation [77]:

$$FRR = \frac{J_{w1}}{J_{w0}} \times 100 \% \quad (2.10)$$

The percentage of oil rejection was calculated using the following equation [77]:

$$R(\%) = \left[1 - \frac{C_{OP}}{C_{OF}}\right] \times 100 \quad (2.11)$$

where C_{OP} and C_{OF} are the concentration of oil in permeate and feed solutions, respectively. The oil concentration in water was measured using a UV-Vis spectrophotometer (Thermo Fisher Scientific GENESYS™ 10) at a wavelength of 300 nm.

2.3.11 Preparation and characterization of oil/water emulsion

The hexadecane-water emulsions were prepared using a handheld homogenizer (Fisherbrand™ 150) stirring at 10,000 rpm. The concentration of prepared emulsion was 1000 mg hexadecane/L and the initial pH of the prepared solution was 5.75. To stabilize the emulsion, tween 80 was used as a surfactant (oil: surfactant weight ratio of 200:3). The stability of the prepared emulsions was assessed by visually monitoring the rested mixture for 24 h. The size distribution of oil droplets in the feed was determined using dynamic light scattering (DLS, ALV / CGS-3 Compact Goniometer, Germany) technique. Fig. 2.1 shows that the oil droplets were in two distinctive radius ranges, where almost 10% of them

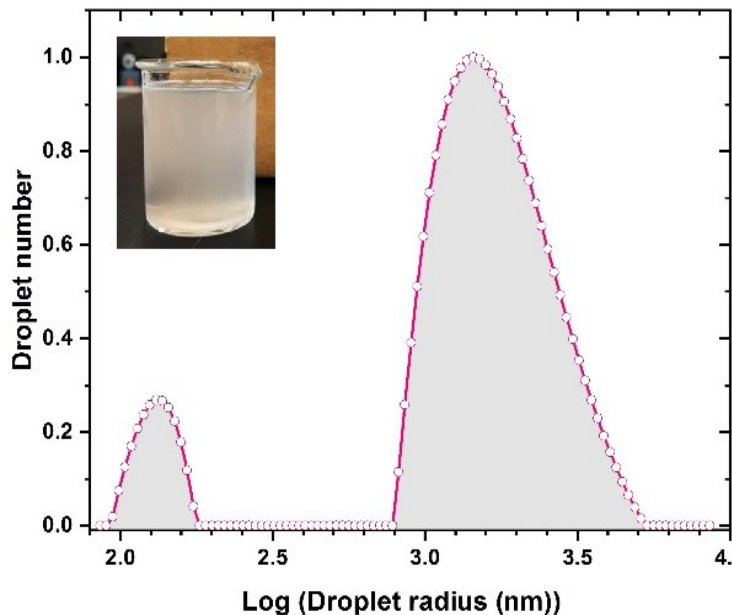


Figure 2.1. The size distribution of oil droplets in the feed solution.

had mean peak positioning at 130.4 nm, and the remaining 90% had mean peak positioning at 1.70 μm .

2.4. Results and discussions

2.4.1. ATR-FTIR results

Fig. 2.2(a) presents the ATR-FTIR spectrum of the pristine and modified PAI membranes. Characteristic imide bands are observed at 1778 cm^{-1} (asymmetrical C=O stretching), 1720 cm^{-1} (symmetrical C=O stretching) and 1378 cm^{-1} (C–N stretching) [78]. The peaks corresponding to amide bonds exist at 1670 cm^{-1} (C=O stretching) and 1500 cm^{-1} (C–N stretching). Moreover, peaks appearing at 1171 cm^{-1} is due to C–O stretching vibration [79]. Other significant characteristic peaks appeared at 1600 cm^{-1} (N–H bending), 1465 cm^{-1} (C–H bending of alkane), 1423 cm^{-1} (O–H bending), 1288 cm^{-1} (C–N stretching of ether), and 1089 cm^{-1} (C–O stretching, alcohol group) [80]. Fig. 2.2 (b) and 2.2 (c) exhibit that, the intensity of peaks appearing at 1465 cm^{-1} (C–H bending, alkane), 1423 cm^{-1} (O–H bending), and 1288 cm^{-1} (C–N stretching, ether) is increased. The intensity increase in the characteristic peaks demonstrates the presence of remaining additives inside the membrane matrix after phase inversion.

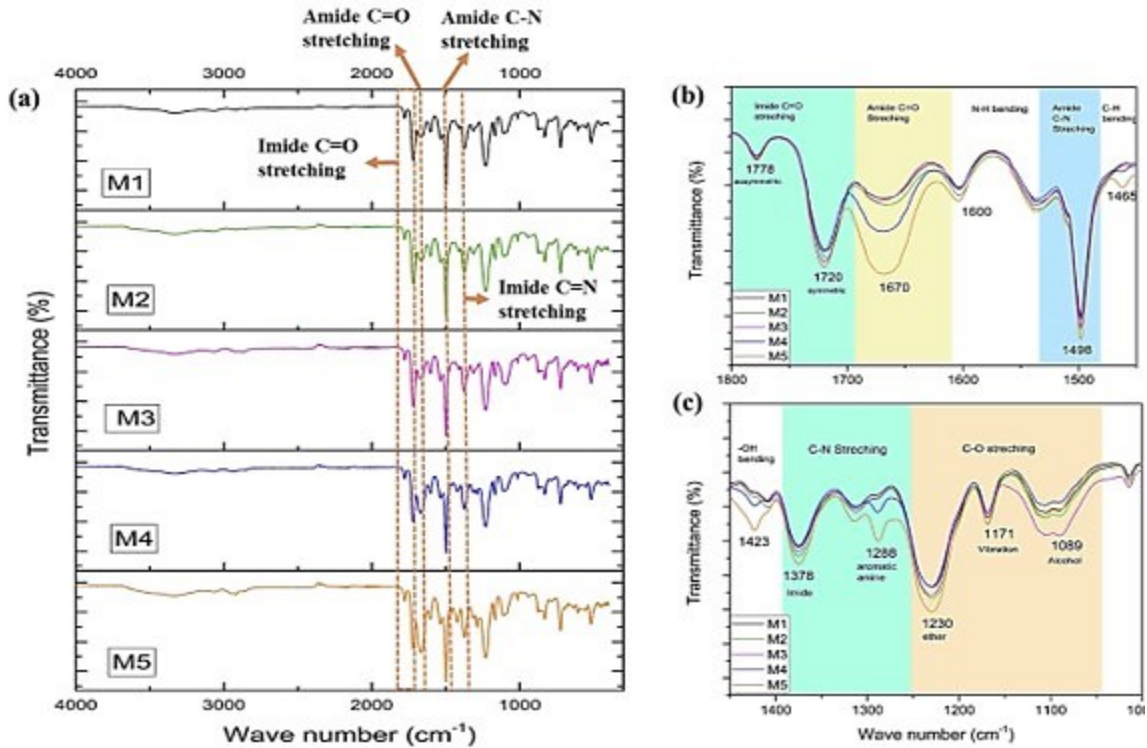


Figure 2.2. (a) ATR-FTIR spectra of the pristine and modified membrane, (b) FTIR spectra at scanning range of 1460-1800 cm^{-1} , and (c) FTIR spectra at scanning range of 1000-1460 cm^{-1} .

2.4.2 Cross-section morphology

The morphological structures of the pristine, as well as modified membranes, are presented in Fig. 2.3. It can be observed that all the membranes except M5 have an asymmetric structure with a thick top skin layer supported by a porous finger-type structure underneath, which is a common internal morphology for membranes synthesized using NIPS technique [79]. In order to evaluate the effect of additives on membrane morphology, it is important to understand the mechanism of membrane formation. When the cast film is immersed in a water bath, polymer precipitation starts because of the imbibition of the non-solvent (precipitant) into the polymer solution. Due to high miscibility between the solvent and non-solvent, phase exchange occurs in several points of top layer being in direct contact with water. The top skin layer is created by excess out-diffusion of the solvent until polymer concentration in the top layer reaches 90%. Beneath the top layer, polymer solidification continues with a slower rate as the skin layer hinders the transport of non-solvent into and the solvent out of the polymer solution [72,81–83]. Skin-type membranes

so-called Loeb-Sourirajan membranes exist in two typical forms: finger-type structure (Fig. 2.3a-d) and sponge-like structure (Fig. 2.3e). The final structure of the membrane is governed by the rate of non-solvent transport from the skin layer to the sublayer. Most of the times, shrinkage stress in the skin cannot be relieved by creep relaxation of the polymer, and this layer ruptures. The points where the skin layer is fractured create the initiation points for the growth of the macrovoids or fingers. When the syneresis and shrinkage effects are overcome (for example by using higher MW additives), the diffusion of the non-solvent through the skin becomes critical, and slow precipitation rate leads to a sponge-like structure. On a microscopic scale, there are regions of higher and lower polymer concentration (polymer-rich and polymer-lean phases), which act as nucleation points for polymer precipitation. These microscopic regions are distributed randomly throughout the cast film and form a sponge-like structure [84].

Wienk et al. proposed another mechanism for the formation of open pores at the skin layer, attributing that to the exchange rate of solvent and non-solvent. During instantaneous de-mixing, polymer experiences a highly non-compatible environment with a lower solubility strength. Due to such quick change, polymer molecules in the top layer tend to diminish their interactions with the non-solvent by clustering together, leading to the formation of open pores on the top layer [83]. Thus, nodules form on the top layer allowing rapid non-solvent intrusion inside the cast film, which results in macrovoids formation within the internal structure of the final membrane. In delayed de-mixing, as mentioned above, non-solvent diffusion through skin layer controls the morphology. Nuclei growth in the top layer is limited, and a large number of small nuclei are formed, which are uniformly distributed throughout the polymer film [85].

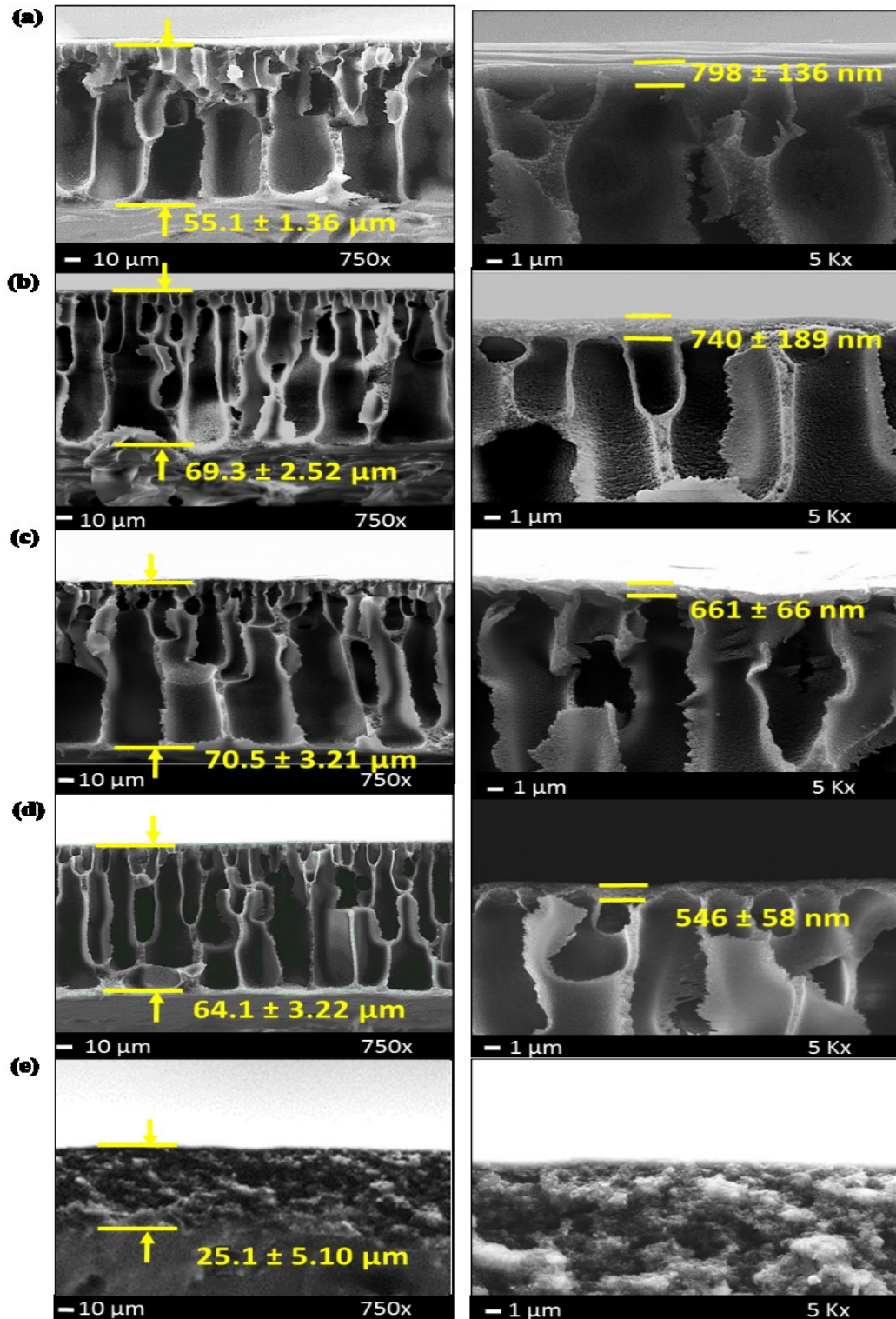


Figure 2.3. Cross-sectional FESEM images of (a) M1, pristine membrane (b) M2, PAI-PEG 0.4 kDa, (c) M3, PAI-PEG 6 kDa, (d) M4, PAI-PVP 10 kDa, and (e) M5, PAI-PEG 360 kDa.

When an additive is added into the polymer solution, it changes the membrane morphology [83]. The morphological difference in these membranes can be explained according to thermodynamic and kinetic characteristics of the polymer solution. When an additive is added into the polymer solution, it interacts with the polymer and solvent in two different ways. It enhances polymer volume fraction and may enhance the interactions between functional groups present in the system [72,86]. The increased polymer volume increases the viscosity of the polymer solution, thereby hinders the kinetics of phase separation, resulting in delayed de-mixing. PEG and PVP, containing hydrophilic functional groups (C=O, -OH), are likely to create a bridge complex with the imide or amide of PAI, which might reduce polymer chain flexibility [83]. Table 2.2 shows the increase in the viscosity of polymer solutions due to the increase in MW of additives.

On the other hand, the additives increase the thermodynamic instability of the polymer solution, which consequently results in instantaneous de-mixing in the coagulation bath [81,82]. As mentioned, this facilitates the formation of macrovoids in the internal structure of a membrane. As a general rule, instantaneous de-mixing leads to the formation of a more porous structure, while delayed de-mixing results in a denser membrane. The kinetic hindrance and thermodynamic enhancement of polymer solution depend on the MW and concentration of the additives [87].

In the case of M1, macrovoids are observed at the bottom section with closely packed smaller pores right beneath of the top skin layer. Some pores are open to the surface, which might be formed due to nodule formation or shrinkage stress on the top layer. The lowest viscosity of M1 suggests that the polymer solution has the lowest kinetic hindrance as compared to others. Therefore, rapid de-mixing has led to the formation of macrovoids. In the case of M2 membrane, suppression of macrovoid is observed, and the thickness of membrane increased. The increase in membrane thickness can be attributed to the swelling of the polymer film by hydrophilic additive [79]. The addition of PEG 0.4 kDa in casting solution increased the kinetic hindrance of the polymer solution, leading to delayed demixing. The elevated kinetic hindrance can reduce the exchange rate between solvent and non-solvent, resulting in suppression of macrovoids. Since PEG 0.4 kDa molecules are small, they might have easily leached out of polymer solution during phase separation, and thus only a small amount of it might be entrapped in the final film.

Formation of large macrovoids in M3 shows the significant effect of the thermodynamic enhancement on membrane morphology. As mentioned earlier, in order to dissolve PEG 6 kDa in the solvent, the additive was heated up at 60°C prior to dissolving polymer/additive mixture. Given that, the polymer solution containing PEG 6 kDa was highly unstable at room temperature, the thermodynamic instability surpassed the effect of kinetic hindrance and led to instantaneous de-mixing. PVP 10 kDa, however, was found to be a macrovoid suppressor [88]. In the case of M4, macrovoid suppression is observed due to the dominant effect of the kinetic hindrance. High MW PVPs do not disentangle easily from the main polymer chains and thus do not create larger pores during phase inversion [83]. In M5 membrane, the viscosity of polymer solution increased enormously, as the entanglement of polymer with PVP 360 kDa macromolecules was notably high. Precipitation took the longest time, leading to the formation of a thinner and denser membrane with a sponge-like structure. Also, PVP 360 kDa macromolecules are hypothesized to relieve the syneresis, shrinkage stress in the skin layer, thereby preventing the rupture of this homogeneous layer. Taking a closer look at Fig. 2.3 shows that the skin layer thickness decreased for all modified membranes. In addition, the skin layer thickness exhibited a declining trend with the increase in the MW of additives.

2.4.3. Surface roughness and wettability

Fig. 2.4 shows the AFM 3D surface topographies of all synthesized membranes. The vertical scales of all AFM images were adjusted to 0.50 μm . As can be observed, the surface of modified membranes became much smoother as compared to the pristine membrane. The arithmetic average roughness (Ra) and the root mean square (RMS) roughness values of the membranes are presented in Table 2.3. The RMS value of M1 membrane (43 ± 2.5 nm) is the highest among all membranes. The RMS values for M2, M3, and M4 are in close range, (14 ± 6.0 nm to 21 ± 3.5 nm). As the polymer solution was highly unstable at ambient condition, the rate of exchange between solvent and non-solvent might have enhanced significantly during phase separation, which has led to a higher variance in roughness. Usually, the hydrophilicity of the additives and the viscosity of the polymer solution are mainly responsible for the variation in surface topography among different membranes [77]. The roughest surface in M1 can be attributed to instantaneous

de-mixing imposed by the low kinetic hindrance of the polymer solution. In the case of modified membranes, the exchange rate between solvent and non-solvent reduced due to the higher viscosity of polymer solution. As a result, a smoother surface was formed owing to less interruption on the top surface. In M5, an enormous increase in polymer solution viscosity resulted in a dramatic increase in top surface stability, making the smoothest surface (10 ± 0.5 nm) among all membranes.

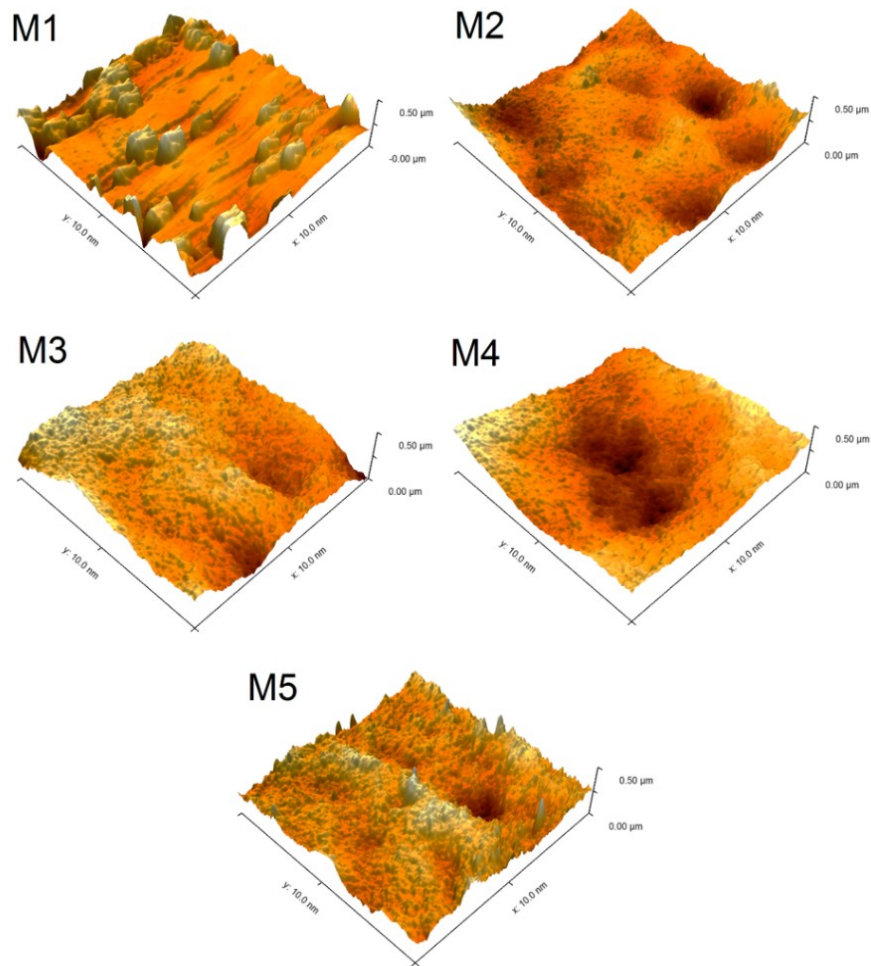


Figure 2.4. AFM 3D images of all synthesized membranes.

Table 2. 3. Surface characterization parameters of all synthesized membranes.

Membranes	OCA (°)	WCA (°)		Roughness (nm)		
		Apparent	Intrinsic	Ra	RMS	r
M1	147 ± 2.5	39 ± 1.86	42 ± 1.86	31 ± 2.5	43 ± 2.5	1.050 ± 0.001
M2	155 ± 5.0	41 ± 0.56	41 ± 0.56	16 ± 3.5	21 ± 3.5	1.002 ± 0.001
M3	160 ± 1.6	41 ± 5.00	41 ± 5.00	11 ± 6.0	14 ± 6.0	1.005 ± 0.001
M4	153 ± 2.2	41 ± 3.50	41 ± 3.50	15 ± 1.8	20 ± 1.8	1.004 ± 0.001
M5	124 ± 1.4	52 ± 0.50	52 ± 0.50	8 ± 0.5	10 ± 0.5	1.002 ± 0.001

The WCA analysis is often conducted to evaluate the membrane surface wettability. In reality, the WCA is partially affected by the roughness of the membrane surface. In previous studies, a surface with higher roughness has been reported to have an elevated wettability [89–92]. Besides surface roughness, surface chemistry has a significant contribution to the wettability of membranes. Surface chemistry is related to the type and amount of hydrophilic/hydrophobic functional groups existing on the membrane surface [92,93]. Hence, the WCA varies due to the synergistic effect of surface physical and chemical characteristics [90,92]. Table 2.3 presents the apparent and intrinsic contact angle of all the synthesized membranes. The intrinsic contact angle ($\theta_{intrinsic}$) is derived from Wenzel equation as follows [90],

$$\cos(\theta_{apparent}) = r \cos(\theta_{intrinsic}) \quad (2.12)$$

where the apparent contact angle ($\theta_{apparent}$) corresponds to the measured contact angle at equilibrium using contact angle analyzer. Intrinsic contact angle corresponds to the contact angle, which excludes the effect of surface roughness. According to the results presented in Table 2.3, no remarkable change in the intrinsic and apparent WCAs was observed for modified membranes. For pristine membrane, apparent WCA was lower than the intrinsic WCA, which can be attributed to the effect of higher surface roughness. The intrinsic WCA for M1 to M4 membranes were found similar, which suggests a similar distribution of polar groups on the surfaces of these membranes. Higher variance in the roughness and WCA of M3 suggests that this membrane has a higher morphological non-homogeneity. The WCA for M5 membrane was the highest, implying the presence of less polar groups on the surface as compared to the rest of synthesized membranes.

2.4.4. Surface free energy

During filtration, the deposition of oil molecules on the surface of a membrane is generally controlled by foulant-membrane interaction [94]. According to the literature, foulant deposition on the membrane surfaces occurs through a combination of hydrodynamic and physicochemical interactions, with the latter being critical for the deposition of foulants on the membrane surface [67,95,96]. The energy related to the affinity between the membrane surface in water and fouling materials (non-polar oil in this study) can easily be described by various surface tension components of the membrane [94]. In this study, membrane surface tension components were calculated using van Oss method by conducting contact angle analysis [66].

Eqn. 2.4 describes the relationship between the free energy of cohesion and surface tension components. The free energy of cohesion is the free energy (per unit area) for interaction between two surfaces of the same material immersed in a solvent (water). If $\Delta G_{SLS}^{TOT} > 0$, the membrane surface attracts water more than the foulant, and thus it is considered hydrophilic. Otherwise, if $\Delta G_{SLS}^{TOT} < 0$, the attachment of foulant molecules to the surface is more facilitated, and the surface is thus considered hydrophobic [89].

The surface tension component data listed in Table 2.4 shows that all synthesized membranes in the present work have higher electron donor components than electron acceptor components, implying that the basic component of the acid-base (AB) interactions controls the polar contribution of the surface free energy. In all cases, non-polar surface tension components constitute the major portion of the total surface tension. The total surface tension component values for all the membranes fall under close range except for M5. It is observed that M5 has a relatively lower electron donor component, meaning that it has a lower polar surface tension component. According to FTIR spectrum (Fig. 2.2 (b)) of the synthesized membranes, the intensity of the hydrophobic C-C bond increased significantly in M5 compared to other membranes. As an outcome, it might have reduced the intensity of polar interaction with water, resulting in a relatively higher WCA and lower polar surface tension component.

The electron donor-electron acceptor components (γ^- , γ^+) of M2, M3, and M4 membranes differ with M1, which may be related to the difference in polar group distribution on the surface of membrane induced by the additives.

Table 2. 4. Non-polar (LW) and polar components (+, -) of the surface tension, the free energy of cohesion (ΔG_{SLS}^{TOT}).

Membranes	Surface tension components (N/m)				ΔG_{SLS}^{TOT} , the total free energy of cohesion (N/m)	
	Total, γ^{TOT}	Nonpolar, γ^{LW}	Positive, γ^+	Negative, γ^-		Polar, γ^{AB}
M1	62.4 ± 0.9	45.50	3.55	20.50	16.79	67.35
M2	63.5 ± 0.8	45.01	4.62	18.50	18.49	67.93
M3	63.4 ± 1.6	45.10	4.35	18.97	18.27	67.74
M4	63.4 ± 0.8	46.50	4.10	17.40	16.89	49.60
M5	59.3 ± 0.3	45.90	3.63	12.40	13.42	-5.33

The free energy of cohesion can provide a quantitative understanding of hydrophobic or hydrophilic interaction between membrane surface and oil [89]. Higher values of ΔG_{SLS}^{TOT} of M1, M2, and M3 suggest that these membranes are more hydrophilic among all synthesized membranes. During filtration of oil emulsion, these membranes are anticipated to prefer water to oil (hexadecane) and their surfaces may reduce concentration polarization through a drastic repulsion of oil. Although the ΔG_{SLS}^{TOT} of M4 is positive its value is less than pristine membrane and the membranes modified with PEG 0.4 and 6 kDa. As M5 is comparatively hydrophobic ($\Delta G_{SLS}^{TOT} < 0$), oil molecules might easily deposit on the surface during emulsion filtration in comparison to other synthesized membranes.

2.4.5. Underwater oil wettability

Underwater oil (hexadecane) contact angle analysis was conducted to assess the propensity of the membranes towards oil fouling. Hydrophilic membranes generally show high underwater oleophobicity. When exposed to water, the hydrophilic surface forms a thin hydration layer that serves as a solid-water interface. Thus, oil basically interacts with the membrane-water interface rather than membrane only. The better the formation of this hydration layer, i.e., the more hydrophilic the surface is, the less is oil adhesion or direct contact of oil with the surface [97,98]. By incorporating hydrophilic groups on the surface of a polymeric membrane, the formation of the hydration layer can be facilitated, and thus,

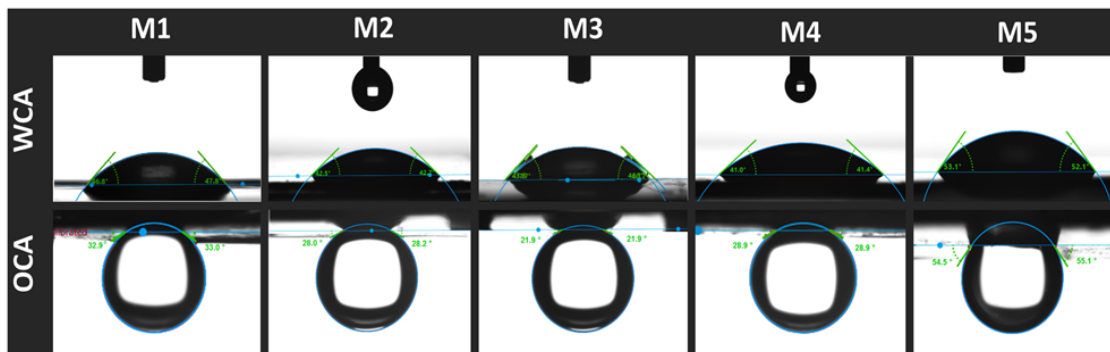


Figure 2.5. Digital images of water and oil underwater droplets over surfaces of different fabricated membranes.

the membranes are endowed with low oil adhesive and better self-cleaning property [99]. According to the literature, the micro/nanoscale roughness and chemical composition of the membrane surface affect the underwater oleophobicity. Thus, the OCA signifies the synergistic effect of the optimized micro/nanoscale surface roughness and active functional groups of membrane surface underwater [98,99].

The average OCA values and visual representation of WCA and OCA for different membranes are presented in Table 2.3 and Fig. 2.5, respectively. The OCA of the pristine membrane was found to be $147 \pm 2.5^\circ$. The OCA value increased to more than 150° for M2, M3, and M4. Therefore, these membranes can be considered as underwater superoleophobic membranes [100]. FTIR spectra of these modified membranes demonstrate the presence of incorporated hydrophilic additives on the membrane matrix. In the event of interaction between oil and membrane surface under water, these additional hydrophilic functional groups might promote the interaction with water, eventually showing a higher OCA. M5 membrane, modified with additive PVP-360000, showed the lowest OCA ($124 \pm 1.4^\circ$). The negative value of the total free energy of cohesion of M5 and its lowest polar contribution (Table 4) clearly explains the reason behind such a reduction in OCA.

2.5. Permeation properties of membranes

The permeation properties of the synthesized membranes are presented in Table 2.5. The additives had a prominent influence on compaction factor (CF), hydraulic permeability, (Hp, $\text{Lm}^{-2}\text{h}^{-1}\text{bar}^{-1}$), porosity (ϵ , %), molecular weight cut off (MWCO, kDa), and average pore size (r_p , nm).

Table 2. 5. Permeation properties (flux and rejection), pore size, and porosity of the synthesized membranes

Membrane	Hp $\text{Lm}^{-2}\text{h}^{-1}\text{bar}^{-1}$	CF	PWF at 0.5 bar	MWCO (kDa)	r_p (nm)	ϵ (%)	Membrane type
M1	625 ± 22	1.85 ± 0.03	343 ± 11	950 ± 19	185 ± 4	52.11 ± 1.14	MF
M2	605 ± 11	1.35 ± 0.04	315 ± 5	800 ± 16	171 ± 3	51.03 ± 0.70	MF
M3	393 ± 7	2.00 ± 0.10	244 ± 3	700 ± 14	161 ± 3	49.97 ± 5.20	MF
M4	500 ± 30	1.56 ± 0.06	295 ± 14	760 ± 15	167 ± 3	50.19 ± 0.57	MF
M5	226 ± 4	1.18 ± 0.006	140 ± 2	500 ± 10	138 ± 2	46.33 ± 2.99	MF

2.5.1. Porosity of membranes

The porosity of a membrane is an important parameter as it influences the permeation rate of water. Porosity demonstrates the ratio of free volume within the membrane matrix to the volume of membrane [79]. The values of porosity of the synthesized membranes are presented in Table 2.5. The porosity of M1 was $52.11 \pm 1.14\%$, which was the highest among all membranes, while M2, M3, and M4 showed slightly lower porosities.

This variation in porosity can be explained by taking a look at the cross-sectional morphology of membranes in Fig. 2.3. M1 had very large voids in its internal structure, while M2, M3, and M4 membranes, showed a slightly less porous structure. Apart from surface roughness and WCA, high variance in porosity is observed for M3. Nevertheless, the porosity results show a minor impact of low MW additives (<10 kDa) on the membrane porosity. However, in the case of M5, porosity reduced to $46.33 \pm 2.99\%$ due to having a compact sponge-like structure as observed in the cross-sectional SEM image (Fig. 2.3).

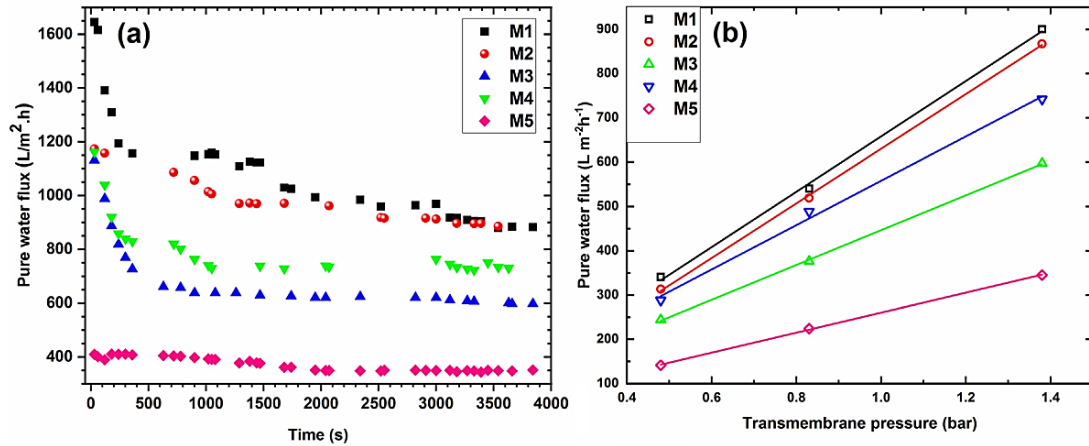


Figure 2.6. Variation of flux for different transmembrane pressure at steady state and (b) Trend of flux decline during compaction.

2.5.2 Compaction factor

Compaction of a membrane due to applied transmembrane pressure is a common feature of MF/UF membranes. During filtration, porous membranes compact due to the collapse of macrovoids at higher pressures. A looser membrane is likely to compact more as compared to a membrane with a denser structure [101]. The CF was calculated as the ratio of initial PWF to steady state PWF [101]. The compaction test was carried out at 1.4 bar. The membranes were compacted until a steady state reached. The compaction time varied between 1 to 3 h for different membranes.

PWF values are plotted against operating time in Fig. 2.6(a) to compare the compaction trend of the synthesized membranes. Likewise, Table 2.5 lists the values of CFs for the synthesized membranes. The highest CF of 2.00 ± 0.10 was observed for M3. It is evident from the SEM image (Fig. 2.3) that M3 contained larger macrovoids compared to other membranes. Under 1.4 bar transmembrane pressure, the collapse of these macrovoids resulted in high compaction of the membrane structure, which manifested the highest CF. The trend of CF followed the order of $M3 > M1 > M4 > M2 > M5$. Although cross-sectional morphology shows that both M1 and M3 membranes contained larger macrovoids, the lower thickness of M1 than M3 might be responsible for the slight reduction in CF. Thinner membrane M1 contained less pore volume than M3 and thus experienced less compaction. Smaller CF values of M2 and M4 membranes than M1 and M3 can be ascribed to their

lower porosities and higher membrane thickness. The very low CF of M5 (1.18 ± 0.006) demonstrates that the tight sponge-like structure of this membrane provided excellent resistance against applied pressure during filtration.

2.5.3. Hydraulic permeability

Before evaluating hydraulic permeability, the membranes were compacted at 1.4 bar until a steady PWF obtained. Upon reaching steady state, PWF was recorded at 1.4, 0.84, and 0.48 bar. The PWFs were plotted against applied pressure in Fig. 2.6(b) and the slope of the linear relationship between PWF and transmembrane pressure was reported as hydraulic permeability. The increase in PWF with transmembrane pressure was found to be linear for all the membranes. It was also found that H_p ($\text{Lm}^{-2}\text{h}^{-1}\text{bar}^{-1}$) decreased with the addition of additives. Table 2.5 presents the values of H_p and steady-state PWF at 0.5 bar for all synthesized membranes. The order of hydraulic permeability is $M1 > M2 > M4 > M3 > M5$, which is correlated with the pore size of membranes. As expected, M1 provided the highest hydraulic permeability and initial PWF ($\sim 625 \text{ Lm}^{-2}\text{h}^{-1}\text{bar}^{-1}$ and $1630 \text{ Lm}^{-2}\text{h}^{-1}$, respectively), while M5 gave the lowest values ($\sim 226 \text{ Lm}^{-2}\text{h}^{-1}\text{bar}^{-1}$ and $400 \text{ Lm}^{-2}\text{h}^{-1}$, respectively). Although M2, M3, and M4 membranes provided a similar initial flux of $1150 \text{ Lm}^{-2}\text{h}^{-1}$, their hydraulic permeability, evaluated at steady state, varied significantly.

Different CFs of these membranes demonstrates the difference in their compaction characteristics, leading to a wide range of variation in final morphology. The variation of pore size at nascent condition is considered as the main reason for the change in compaction characteristics.

2.5.4. Average pore size of membranes

In this study, the MWCO experiment was carried with three MW of dextran including 150, 250, and 500 kDa. First, the membranes were compacted using the method described in the previous section and the dextran rejection was measured at 0.48 bar. The rejection (%) results were plotted against the MW of dextran for each membrane. The curves were then extrapolated to achieve 90% rejection of dextran of a particular MW. As presented in Table

2.5, the average pore size of the membranes follows the order of M1>M2>M4>M3>M5, which is in good agreement with the Hp results.

2.6. Oil removal experiments

Performance of membranes for oil/water separation is typically influenced by two mechanisms, size exclusion (i.e., sieving) and selective wettability. The former mechanism is ruled by pore size distribution and porosity, and the latter is governed by the hydrophilicity, roughness, and functional groups of the membrane surface [102–105]. In addition to these factors, operating conditions such as transmembrane pressure, oil concentration, pH of the feed solution, and feed flowrate play crucial roles in the permeate flux and oil removal efficiency [101]. Hydrodynamic forces, such as transmembrane pressure, play an important role in permeate flux decline. As pressure increases, at a critical point, the applied pressure overcomes the capillary pressure, which prevents oil from clogging the pores, and afterward, oil molecules get squeezed into the pores [101]. Clogging of pores builds up an additional barrier against water passage, which sharply declines the water permeation rate. It was shown that membranes with larger pores are rapidly fouled by macron/submicron size oil droplets [101–104]. The underwater oleophobicity and pore structure of a surface can also influence the formation of the oil film. Oil molecules deposits on an oleophilic membrane due to the interaction between oleophilic groups and oil molecules, which subsequently results in membrane fouling. In this section, the permeation properties and fouling resistance of synthesized membranes are evaluated and compared. Oil/water separation experiments were carried out at similar operating conditions (initial flux, temperature, and feed flow rate) and feed solution properties (pH and oil concentration) to solely correlate the performance of the membranes with their physicochemical properties, such as surface energy, roughness, pore size, porosity, and internal morphology [106,107]. The water flux regeneration capability of synthesized membranes was also evaluated and compared.

2.6.1. Comparison of membranes

Prior to emulsion filtration, the membranes were compacted at 1.4 bar to reach a steady PWF. The initial PWF was fixed at $300 \text{ Lm}^{-2}\text{h}^{-1}$ for all membranes by adjusting the transmembrane pressure. The range of applied pressure was between 0.45 to 0.53 bars for

all membranes, except for the tightest membrane, M5, whose transmembrane pressure was set to 1.4 bar. The trend of flux decline for all membranes is presented in Fig. 2.7. Membranes modified by lower MW additives, (M2, M3, and M4) demonstrated almost 13% improvement in FD (%) compared to the pristine (M1) membrane. The reason behind such observation could be the improvement in the membrane morphology and underwater oleophobicity of the membranes. These modified membranes demonstrated higher underwater oleophobicity ($\text{OCA} > 150^\circ$), smoother surfaces, and smaller average pore size compared to the pristine membrane. At the beginning of experiments, when the effect of concentration polarization is trivial, the initial drastic decline in flux can be attributed to pore blocking. In the later stage, flux declines due to the development of a concentration polarization layer, as well as, the formation of an oil film on the surface, which reduces the active surface area for water transport [101]. As modified membranes had smaller average pore sizes, the initial decline was less than the pristine membrane.

Moreover, due to improvement in their underwater oleophobicity, the attachment of oil to their surface is minimized, resulting in a relatively steadier water flux in less than 200s. Over time, these membranes showed a superior permeation rate as high as $210 \text{ Lm}^{-2}\text{h}^{-1}$ at a very low operating pressure. M5 membrane, on the other hand, suffered 23% FD (%) as compared to the pristine membrane, which seems to be inconsistent with its tight internal

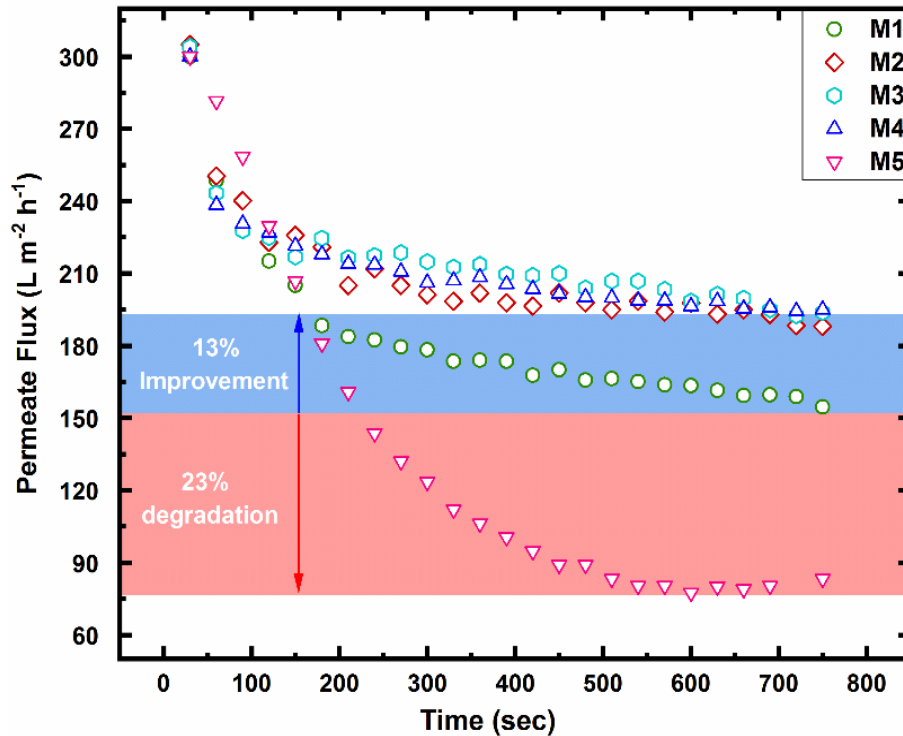


Figure 2.7. Permeate flux decline over time due to oil fouling for all synthesized membranes.

structure. Due to its significantly lower underwater oleophobicity, oil macromolecules strongly adhered to M5 membrane surface or internally blocked the pores. Severe oil fouling considerably restricted water passage, leading to the highest FD (%) among all membranes.

2.6.2. Reusability of membranes

To investigate the reusability of the synthesized membranes, oil rejection experiments were conducted for three consecutive cycles at 0.48 bar pressure with feed solution of constant concentration and pH. The normalized permeation flux with initial PWF was plotted against operating time in Fig. 2.8(a). As can be seen in Fig. 2.8(a), the FD follows the trend of M1>M2>M4>M3>M5 in the first cycle. Fig. 2.8(b) presents the values of FD in all three cycles. M1 had the highest decline in permeate flux (47%) possibly due to its bigger average pore size. The decline in permeate rate improved by 4%, 18%, 10%, and 25% for M2, M3, M4, and M5 membranes, respectively. Fig. 2.8(c) shows that all membranes, except for M5, recovered more than 98% of water flux, which demonstrates excellent regeneration of membranes in the first cycle. In the next two cycles, the FD decreased to

51% and 53% for M1, while it remained almost constant or declined very slightly for the modified membranes. Although M1 membrane possesses good underwater oleophobic property ($147^\circ \pm 2.5$), its surface is comparatively rougher than that of modified membranes. The accumulated oil on the cavities of rough structure and inside the pores might be difficult to remove by simple washing. More severe flux decline in the second cycle (Fig. 2.8c) confirms this hypothesis. On the other hand, M2, M3, and M4 membranes were more oleophobic and had comparatively smoother surfaces compared to the pristine membrane. The combined effect of these properties improved anti-oil adhesion property during filtration, which resulted in better flux recovery. Among all membranes, M3 showed excellent consistency in terms of flux recovery for all three consecutive cycles. A likely explanation is its superior oleophobic property ($\text{OCA}=160^\circ \pm 1.6$). M5 Membrane showed a decline in FRR in all three cycles. The negative ΔG_{SL}^{TOT} (-5.33 ± 0.3) and low OCA ($124^\circ \pm 1.4$) suggest that this membrane is more oleophilic as compared to the other synthesized membranes. During filtration, oil molecules could strongly adhere to the membrane surface and/or within pores, which caused washing less efficient in M5. Therefore, lower water flux recovery was observed in all three cycles, representing more oil fouling tendency of M5 as compared to other membranes.

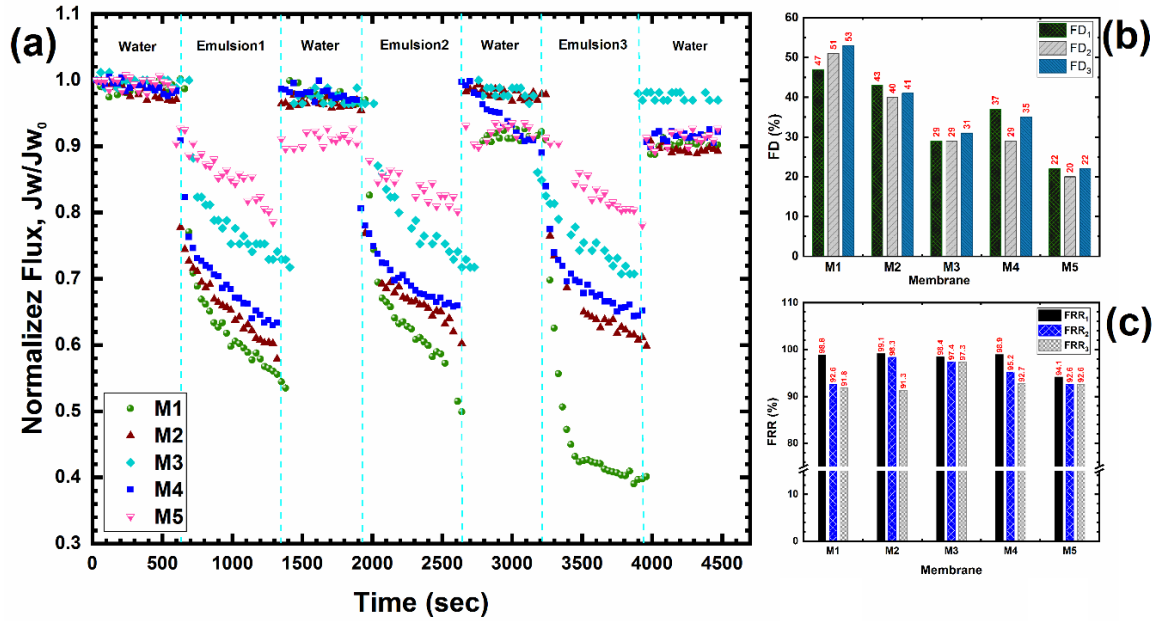


Figure 2.8. (a) Variation of normalized flux (J_w/J_{w_0}), (b) Percentage of flux decline, and (c) Flux recovery ratio at 0.5 bar transmembrane pressure for three consecutive cycles of oil/water emulsion treatment.

Fig. 2.9 presents the percentage of oil rejection in three cycles for all the synthesized membranes. The membranes showed rejections above 98% for hexadecane. Only in the case of the pristine membrane, rejection declined slightly in the third cycle. Membrane swelling or relaxation of polymer chains after washing can be considered as a possible reason for such observation [101]. A loose structure is typically more prone to swelling than a dense structure [101]. Hence, the relaxation of M1 polymer chains in the third washing cycle was possibly more severe than other membranes. A slightly swollen structure allowed additional oil molecules to pass through the membrane.

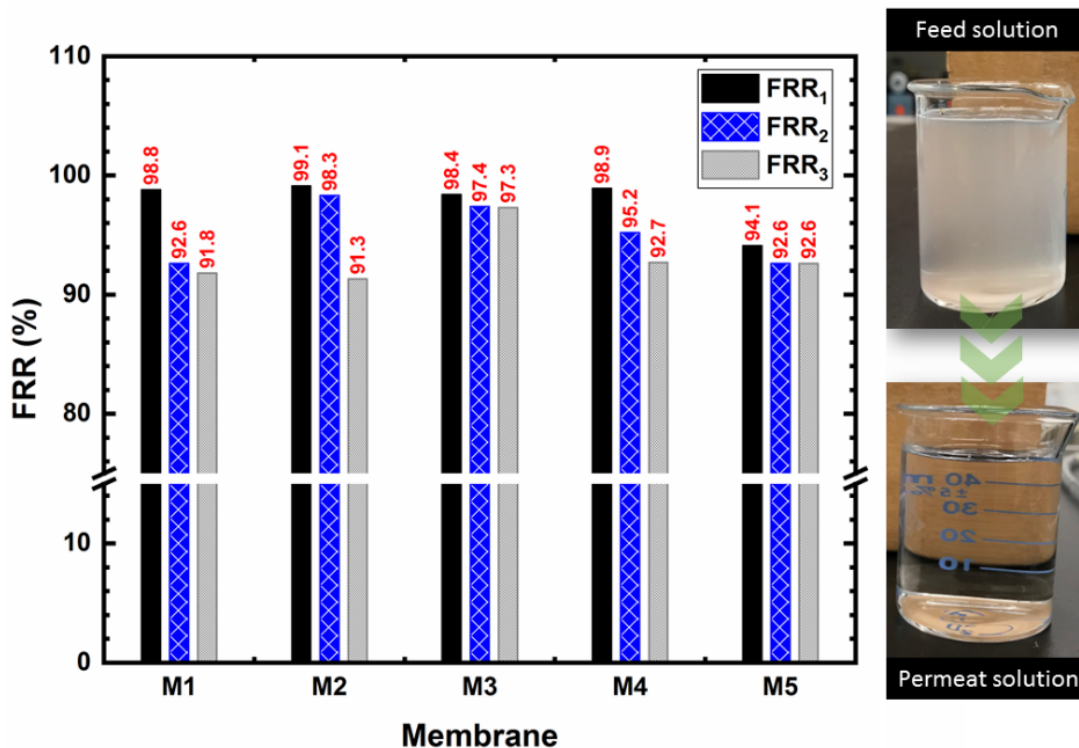


Figure 2.9. Oil rejection in three consecutive emulsion treatment cycles and optical pictures of feed and permeate solutions.

2.7. Conclusion

In this study, underwater superoleophobic PAI MF membranes were fabricated by non-solvent induced phase inversion (NIPS) technique for the treatment of oil-in-water emulsion. The synthesized membranes exhibited high hydraulic permeability ranging from 226 to 625 ($\text{Lm}^{-2}\text{h}^{-1}\text{bar}^{-1}$). The membrane exhibited excellent oil removal efficiency (98%) at a permeation rate of 210 ($\text{Lm}^{-2}\text{h}^{-1}$) when a very low transmembrane pressure of 0.48 bar was applied. In addition, hydrophilic additives (PEG 0.4 and 6 kDa and PVP 10 kDa) incorporated into the membranes prevented rapid flux decline and enhanced regeneration capacity of the membranes. Moreover, the use of additive enabled tuning of the surface roughness and provided anti-compaction properties through manipulating the thermodynamics and kinetics of polymer solution. Creating physical heterogeneities to the surface of PAI can potentially improve their oil fouling property and regeneration capacity even further. In summary, the inherent low-oil-adhesion and self-cleaning properties of PAI membranes make it a superior candidate to conventional PES and PSF membranes for

oily wastewater treatment. PAI can also be used as a new platform for the fabrication of superhydrophilic and underwater superoleophobic membranes without a need for cumbersome chemical grafting methods. This study opens up a new paradigm for the application of PAI MF membranes in oily wastewater treatment in a broad range of commercial processes.

Chapter 3: Layer by layer assembly of polyamide Imide (PAI) membrane by electrostatic deposition of polyelectrolytes for SAGD produced water treatment.

3.1 Introduction

Steam assisted gravity drainage (SAGD) is a thermally enhanced heavy oil recovery method for producing bitumen and heavy crude oil widely adopted by oil sands industries in Alberta, Canada. In the SAGD process, steam is injected underground to reduce the viscosity of bitumen. Steam is injected through injection well placed above production well which causes bitumen to melt and flow down in the production well. The heated liquid bitumen and steam condensate reaches down to the production well located beneath the injection well. The bitumen is then pumped out to the surface where water and bitumen are separated and later the water is treated for using as the boiler feed water [108]. Current treatment processes include warm lime softening (WLS) and ion exchange (IX) resins, which do not provide any treatment for the TDS or dissolved organic matter (DOM). Typical SAGD water composition after conventional treatment is summarized in Table 3.1 [19]. This harsh water, containing a high mineral and DOM concentration, causes scaling of boiler tubes. The boilers currently used in the SAGD operations are once through steam generators (OTSGs), which are able to handle BFW of relatively high amount of TDS (< 8000 ppm) and Ca/Mg/Si than conventional drum boilers [109]. As the feed water used for OTSGs is of very poor water quality, OTSGs typically produce only a low-quality steam (75-80%).

The produced steam is separated from the liquid at the exit of OTSG and is sent into the reservoir. The separated liquid having high concentration of dissolved solids and organics is known as boiler blow down water (BBD). A portion of BBD is sent to the WLS and the remainder is disposed.

The OTSG feed water, namely BFW, can create numerous problems like boiler failures due to the deposition of silica, divalent ions, and organic matter on the boiler tube walls and clogging of injection wells [110]. Fouling of the boiler tubes frequently results in periodic shutdown in bitumen production due to plant overhaul for cleaning and

maintenance [111]. To reduce disposal rate of BBD, evaporators are sometimes used as a downstream BBD recovery process, which are highly energy intensive. Deposits analyzed from fouled tubes contains high levels of organic carbon and Ca/Mg/Si. Thus, to prevent fouling of OTSGs and to reduce the volume of disposal, oil sands industries are seeking alternative water treatment technologies.

Membrane based separation processes are widely used for produced water treatment due to their capacity for producing high quality water, lower operating cost and lower energy consumption. For the separation of a contaminants of relatively lower size and molecular weight such as silica, DOM, and salt, the use of nanofiltration (NF) and reverse osmosis (RO) membrane have been reported [112]. In order to improve the operation of the current OTSGs, a membrane-based treatment of SAGD produced water would provide high-quality BFW, which might reduce fouling of OTSGs significantly [107].

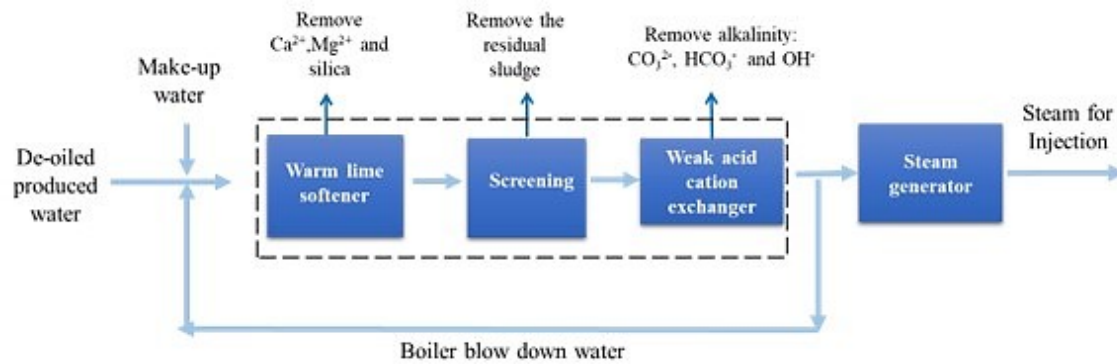


Figure 3.1. Process flow diagram of a typical SAGD process.

Table 3.1. Specification of BFW of SAGD operation.

Parameter	Units	Specification
Conductivity	mS/cm	1.8-2.2
TDS	mg/L	1800- 2000
pH	-	9.8-10.5
DOM	mg/L	450-620
Silica	mg/L as SiO ₂	30-40
Calcium	mg/L	0.4 – 0.5
Iron	mg/L	0.2 – 0.3

It is a well-known fact that fouling of membranes is the primary challenge for its practical application. Surface modification of polymeric membranes is a method to alter membrane surface properties, and thus mitigate fouling. Generally, hydrophilic polymers (neutral or charged), zwitterionic polymers, amphiphilic polymers, biopolymers, and nanomaterials, are employed for surface modification for increasing selectivity and anti-fouling property towards a particular/group of foulant. Among all membrane modification techniques, such as chemical grafting and plasma treatment, layer-by-layer (LbL) assembly of polyelectrolyte is a simple and versatile method to alter pristine membrane property. LbL assembly is driven by molecular interaction, such as electrostatic interactions, hydrogen bonding, charge-transfer interactions, host-guest interactions, biologically specific interactions, coordination interactions, covalent bonding, stereo complexation, and surface sol-gel process [113].

Compared to conventional membrane modification techniques, LbL assembly is more environmentally friendly as it utilizes the deposition of water-soluble polyelectrolytes [1]. The LbL assembly method simply requires alternative deposition of polycations and polyanions on the surface of a porous substrate to form multi-layers until the desired selectivity and permeation characteristics are achieved. In this procedure, the thickness of the deposited layer can be effectively controlled in nanoscale, and the composition of the top surface can also be changed. Nevertheless, the increase in hydraulic resistance increases due to deposited layer by the LbL assembly, which can also be regulated by controlling the LbL thickness [1].

Most of the polyelectrolyte pairs reported in previous research include poly (allylamine hydrochloride)/polystyrenesulfonate (PAH/PSS), poly(vinylamine)/poly(vinyl sulfate) (PVA/PVS), poly(ethyleneimine)/PVS (PEI/PVS), PEI/PSS, PAH/PVS), PAH/dextran sulfate (PAH/DEX), poly(diallyldimethylammonium chloride)/PSS (PDADMAC/PSS), poly(4-vinylpyridine)/PSS (P4VP/PSS), chitosan/polystyrenesulfonate (Chi/PSS), poly (acrylic acid)/poly(ethylenimine) (PAAc/PEI), PEI/alginate acid (PEI/Alg), PDADMAC/PAAc, Chi/Alg, and Chi/PAAc [114]. These polyelectrolytes have high density of hydrophilic functional groups, which enables the formation of a closely packed

LbL-assemblies. Presence of hydrophilic functional groups on the membrane surface plays a crucial role in mitigating membrane fouling [113].

LbL assembly of polyelectrolytes was initially proposed by Decher, who demonstrated the formation of 100 thin layers of alternating polyanions and polycations on the surface of a silicon substrate in the early 1990s by consecutively alternating adsorption of anionic and cationic polyelectrolytes on charged surfaces [115]. Later Numerous research have been conducted on improvement of LbL assembly method by adjusting the deposition conditions (pH, concentration, deposition time) [116,117]. The modified membranes by LbL assembly method showed reasonably improved performance in terms of various targeted purposes, such antifouling property and separation performance [116,117]. Lajimi et al. deposited chitosan/alginate polyelectrolyte up to 15 bilayers on cellulose acetate (CA) membranes and found almost 100% divalent salt retention [118]. Tieke et al. deposited 30 bilayer of PVA and PVS polyelectrolytes and exhibited > 90% rejection of divalent ions [119]. Besides the organic polymers, inorganic nanoparticles can also be deposited on the surface of MF or UF membranes via LbL assembly. Diagne et al. modified commercial polyethersulfone (PES) membranes by LbL assembly of PSS and PDADMAC polyelectrolytes, and integrated silver nanoparticles onto the surface. The film was found to be stable and the modification significantly reduced organic and biological fouling [120]. Researchers also fabricated NF membranes via LbL self-assembly method, and investigated the removal of dye or natural organic matter (NOM), and monovalent and divalent ions [121–123]. Wang et al. assembled graphene oxide (GO) with polycation to form a multilayer on polyacrylonitrile substrate. The polycation/GO multilayer membrane rejected >99% of methyl blue molecule and provided $6.42 \text{ kgm}^{-2}\text{h}^{-1}\text{bar}^{-1}$ - water permeability[124].

The surface functionality of a substrate plays a significant role in effective deposition of polyelectrolytes having opposite charges. Different polyanions and polycations may deposit on a substrate with different rates depending on the surface charge density. A substrate which have a high negative charge would alleviates the electrostatic deposition of positively charged polyelectrolyte and consequently shortens the deposition time. In this work, polyamide imide (PAI) membrane was selected as a substrate, for the first time, due

to its superior hydrophilic property. LbL assembly was carried out using polydiallyldimethylammonium chloride (PDADMAC) and polyacrylic acid (PAA) as oppositely charged polyelectrolytes in order to improve antifouling and rejection performance of PAI membranes.

3.2 Materials and Methods

3.2.1 Materials

PDADMAC (Mw) 200-350 kDa and PAA (Mw) 450 kDa, were purchased from Sigma Aldrich. Deionized water (Milli-Q, conductivity of 18.2 M Ω cm) was used for membrane rinsing and preparation of polyelectrolyte solutions. SAGD BFW water used as a foulant obtained from a SAGD treatment plant located in the Athabasca oil sands region of Alberta, Canada. Samples were collected, shipped in sealed containers, and were kept in an inert atmosphere with a nitrogen blanket.

3.2.2 Layer by layer membrane modification

PAI membranes with the MWCO of 750 kDa were synthesized on a polyester fabric in lab by the non-solvent phase separation (NIPS) method, described in chapter 2, and used as a substrate. PAI support (M1) was attached in a frame and 20ml 0.01 wt% PDADMAC solution was poured onto the active side of membrane. The deposition carried out for 5 minutes followed by submerging in a beaker of 1 L water for washing. Afterwards 20 ml 0.01 wt% PAA was deposited for another 5 minutes followed by washing. The depositing and washing process were repeated for making two (M3) and four bilayers (M4). The successful deposition of polyelectrolytes was checked with zeta potential analyzer.

3.2.3 Crossflow membrane filtration setup

The schematic view of the crossflow membrane filtration setup is shown in Fig. 3.2. The maximum operating pressure allowed of the setup is 200 psi which is provided by a diaphragm pump (HydraCell) of maximum flow 6.8 LPM. The effective filtration area was 20.6 cm². In all experiments, feed flow rate was set at 1.6 LPM. A bypass valve and a back-pressure regulator (Swagelok) were used to adjust the feed flow rate and the transmembrane pressures. A weighing balance (Mettler Toledo EL4001) was used to measure the permeate flow rate. The pH of BFW was measured by a Mettler Toledo

(SevenMulti S47) pH meter. The weight of permeate was transferred every 15 seconds interval to a computer through Mettler Toledo software.

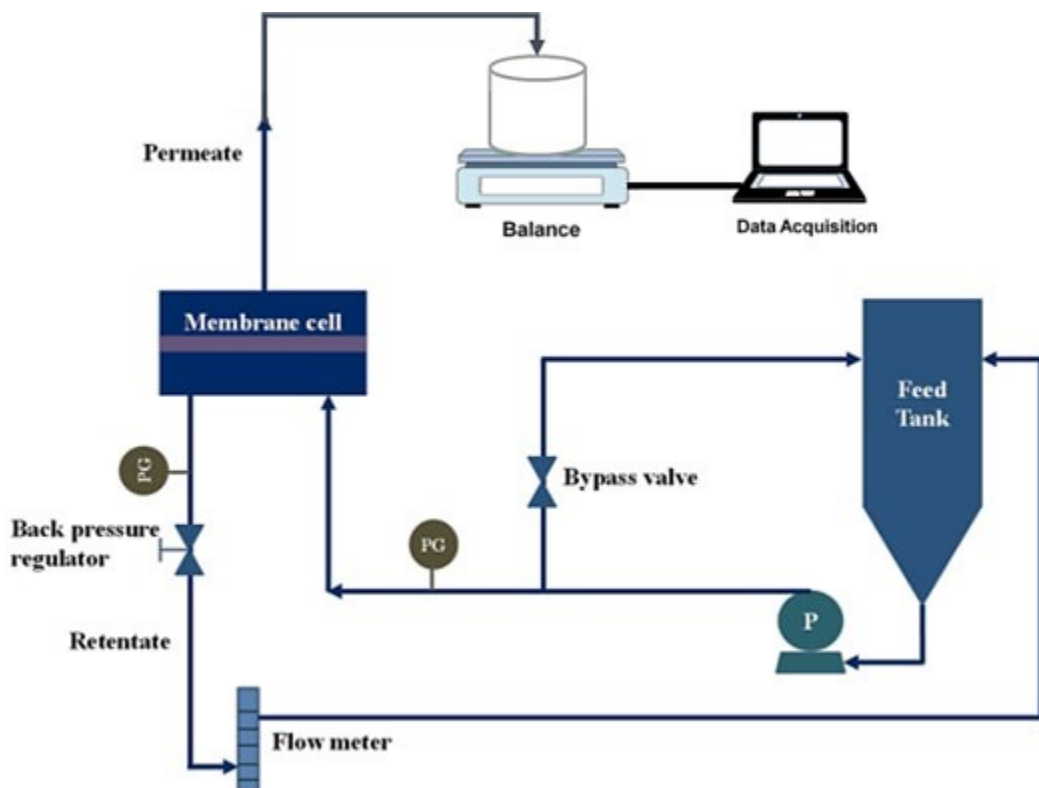


Figure 3. 2. Schematic of Crossflow filtration set-up. Reprinted with permission from [107].

3.3 Characterization techniques

3.3.1 Experimental methodology

Prior to the test, the membranes were compacted at 40 psi to reach a steady pure water flux (PWF). The filtration of BFW was carried out at $140 \text{ L m}^{-2} \text{ h}^{-1}$ initial flux for 1 hr. The same initial flux was achieved by adjusting the transmembrane pressure for different membranes. Feed flow rate was maintained at 1.6 LPM. The permeate was collected and the rejection of organic compounds was measured using UV-Vis spectrophotometer (Thermo Fisher Scientific GENESYS™ 10) at a wavelength of 290 nm. After filtration the membranes were washed with pure water for four minutes, afterwards the washed water was discarded from the setup and this cycle was repeated for two more times. The washing was performed at zero transmembrane pressure. After washing the PWF was recorded. The

percentage of flux decline (FD), flux recovery ratio (FRR) and rejection percentage of organic matter (R) were calculated using the following equations. In the following equations J_{W0} is initial PWF, J_W is permeate flux after 1 hr, and J_{W1} is PWF after washing.

$$FD = 1 - \frac{J_W}{J_{W0}} \times 100 \quad (3.1)$$

$$FRR = \frac{J_{W1}}{J_{W0}} \times 100 \quad (3.2)$$

$$R(\%) = \left[1 - \frac{C_{permeate}}{C_{Feed}} \right] \times 100 \quad (3.3)$$

Where, $C_{Permeate}$ and C_{Feed} are the concentrations of organic material in permeate and feed, respectively.

3.3.2 Field emission scanning electron microscope-energy dispersive X-ray (FESEM-EDX)

The membranes were sputter coated with a thin film of chromium. Surface images of the membranes were obtained using JEOL 6301F FESEM. All membranes were imaged at a magnification of 20,000 times. FESEM provides qualitative information on the deposition of foulants on the membrane. Semi-quantitative elemental analysis was done via a PGT IMIX EDX system with 135 eV resolution.

3.3.3 Zeta potential measurement:

The surface zeta potential of the fabricated membranes was measured using Surpass3 analyzer (Anton Paar, Graz, Austria). This device evaluates the surface zeta potential based on streaming potential and streaming current measurements. The zeta potential values were determined at pH 7.0 and 25 °C using 0.001 M KCl solution. The zeta potential of polyelectrolyte solution was measured using Malvern Zetasizer Nano ZS90. This device measures zeta potential using Laser Doppler Microelectrophoresis.

3.3.4 Contact angle

The wettability of the samples was characterized using Kruss GmbH contact angle analyzer (Hamburg, Germany), following the similar procedure described in chapter 2.

3.4 Results and discussion

3.4.1 Surface charge

Membrane surface charge is a critical parameter for selecting an appropriate membrane for a particular treatment process [67]. The more negative surface charge is proven to reduce fouling by both organic and inorganic materials which are mostly negatively charged. A polymeric membrane acquires surface charge in an aqueous medium by two mechanisms: dissociation of membrane functional groups or adsorption of cation and anions on the membrane surface. This charged membrane surface repels co-ions and attracts counterions and affects the ionic distribution at the membrane-media interface and consequently, forms an electrical double layer on the surface [67].

The potential created at the boundary between the surface and non-movable parts of the double layer, normally referred to as the shear plane, is the zeta potential (ξ). Streaming potential or zeta potential is measured by applying pressure gradient in tangential flow mode at the membrane surface. When the motion is applied, the ions within the double layer will partly strip away. This creates a potential drop (ΔE) (dependent on pressure gradient) at the end of channel. Then the zeta potential can be calculated using the Helmholtz–Smoluchowski equation.

$$\xi = \frac{\Delta E}{\Delta P} \frac{\eta \lambda_0}{\varepsilon_0 \varepsilon_r} \quad (3.4)$$

Here, η is the viscosity of the electrolyte solution, ε_0 the permittivity of vacuum, ε_r is the dielectric constant of the electrolyte, and λ_0 is the specific conductivity of the electrolyte within the pores.

Fig 3.3(a) shows the zeta potential of polyelectrolyte solutions over the pH range of 3-8. As can be observed, PDADMAC is positively charged over the whole pH range and would easily deposit on a negatively charged substrate. Likewise, at all pH values PAA disassociates into negatively charged functional groups and would deposit on positively charged surface.

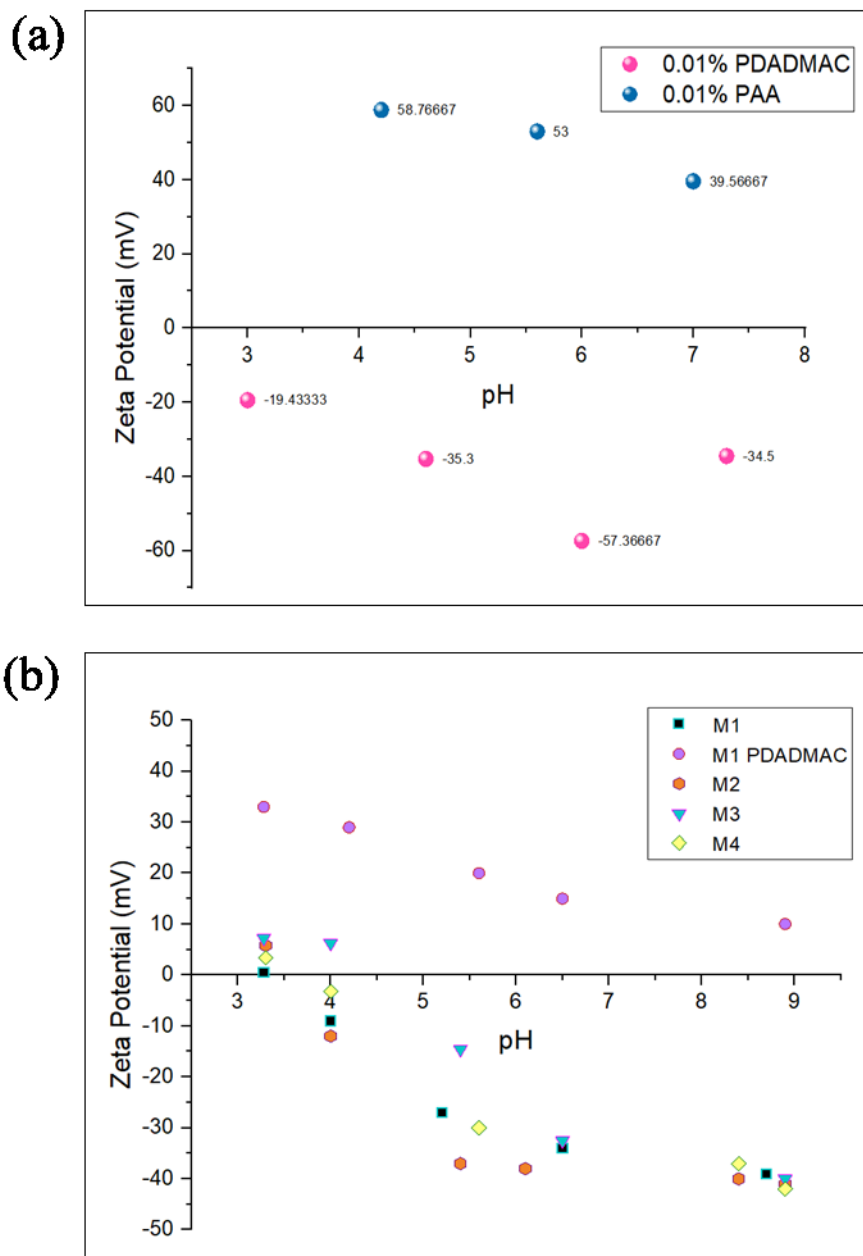


Figure 3.3. (a) Variation of zeta potential due to deposition of PDADMAC and PAA onto membrane surface, (b) Zeta potential of polycation PDADMAC and polyanion PAA.

Fig 3.3(b) presents the zeta potential of pristine and coated membranes. Bare PAI membrane is negatively charged in all pH values due to presence of C=O, C-O functional groups in its structure. The positive value of zeta potential for M1-PDADMAC, over the entire pH range, indicates the successful deposition of PDADMAC on the membrane surface. Similarly, M2 curve shows the successful deposition of negatively charged PAA.

The negative zeta potential of M3 and M4 also suggests that the bilayers have successfully been formed. In all cases, with increasing pH the zeta potential became more negative. Elimelech and Childress conducted the effect of pH on zeta potential for thin film polyamide membranes at various concentration of NaCl, Na₂SO₄, CaCl₂ solutions. In all cases, the zeta potential of the membranes became more negative with increasing pH of electrolyte solution [125]. At pH values more than the isoelectric point (IEP), the acid groups present in membrane surface disassociates and the surface becomes more negatively charged. When membrane is coated with a substance which has high charge density, specifically acidic functional groups such as carboxylic (-COOH) and hydroxyl groups (-OH), the membrane surface becomes rich in ionizable functional groups. With increasing pH, these groups are deprotonated to -COO⁻ and -O⁻ negative groups and increase the negative charge concentration over the membrane surface [126].

It is worth noting that no distinct variation in zeta potential of membrane samples is observed. A likely explanation is that zeta potential measurement does not provide the amount of charge present in the coating layer, rather it measures the potential created at the shear plane.

3.4.2 FESEM-EDX

Fig. 3.4 shows FESEM images and the EDX analysis of the fabricated membranes. For all the membranes, carbon, nitrogen and oxygen are detected in EDX chemical elemental analysis. The presence of Na and Cl peaks could be due to residual NaCl on the membrane surface during washing step. The intensity of carbon peak was found the highest in M1, which gradually reduced in the case of bilayer membrane. Accordingly, the intensity of nitrogen and oxygen increases due to LbL assembly deposition. This can be attributed to the addition of amin (-NH₂) and hydroxyl acid (-COOH) functional groups obtained from the utilized polyelectrolytes. The findings from EDX analysis is in line with the findings from FTIR spectra, which suggests an increase in hydrophilic functional groups in the LbL assembly membranes.

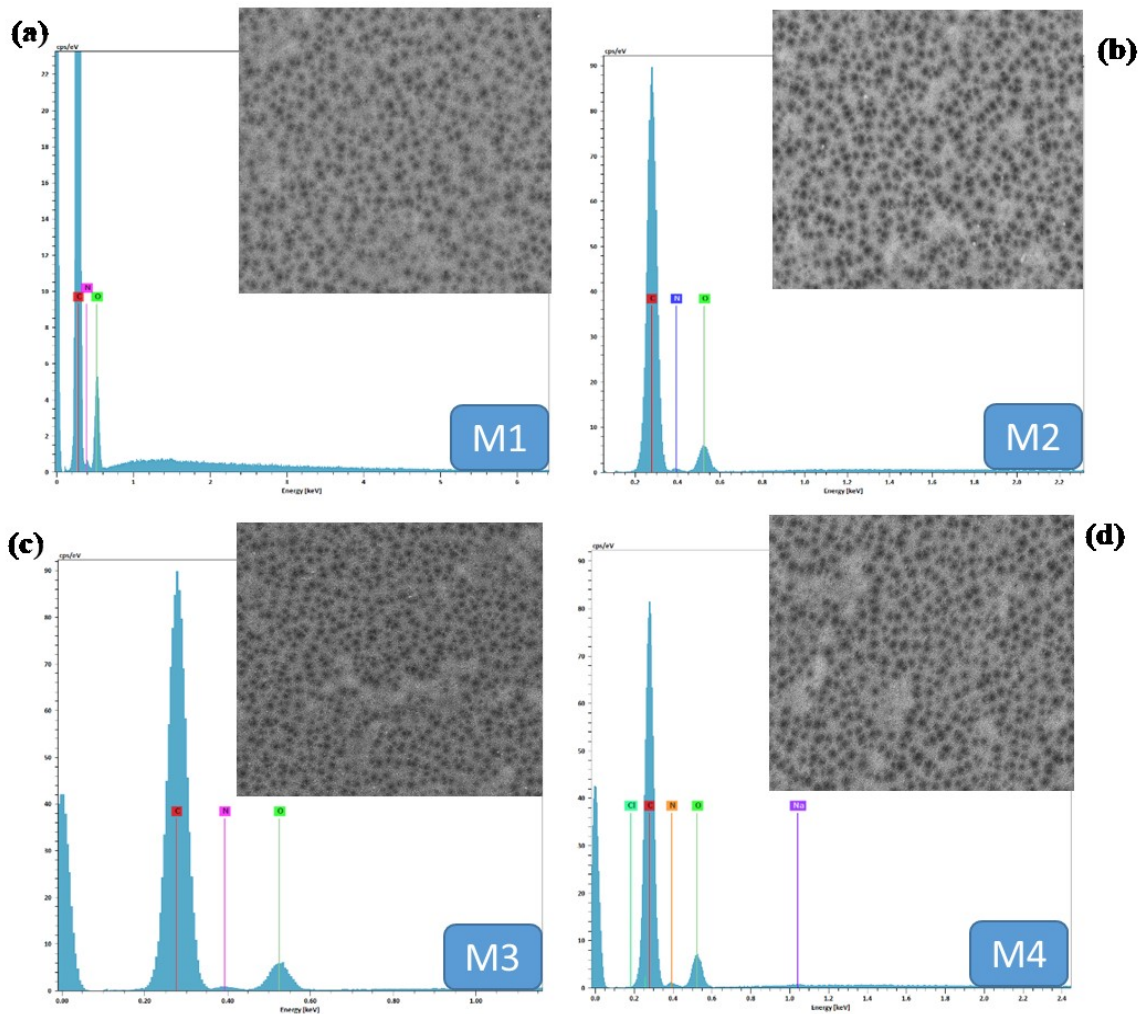


Figure 3. 4. FESEM-EDX of all the membranes before filtration.

3.4.3 ATR-FTIR results

Membrane samples were scanned from wave number range 390 to 4000 cm^{-1} before and after filtration. Figure 3.5 represents the ATR-FTIR spectra of bare and bilayer PAI membranes over scanning range of 1200 to 2000 cm^{-1} . Since the polyelectrolytes (PDADMAC and PAA) and the pristine polymer contain similar molecular groups no new peaks are detected. The intensity increase of characteristic peaks occurring at 1778 cm^{-1} (asymmetrical C=O stretching), 1720 cm^{-1} (symmetrical C=O stretching) and 1378 cm^{-1} (C–N stretching) and amide peaks observed at 1670 cm^{-1} (C=O stretching) and 1500 cm^{-1} (C–N stretching) could be attributed to the deposition of polyelectrolytes on the surface of the PAI membranes.

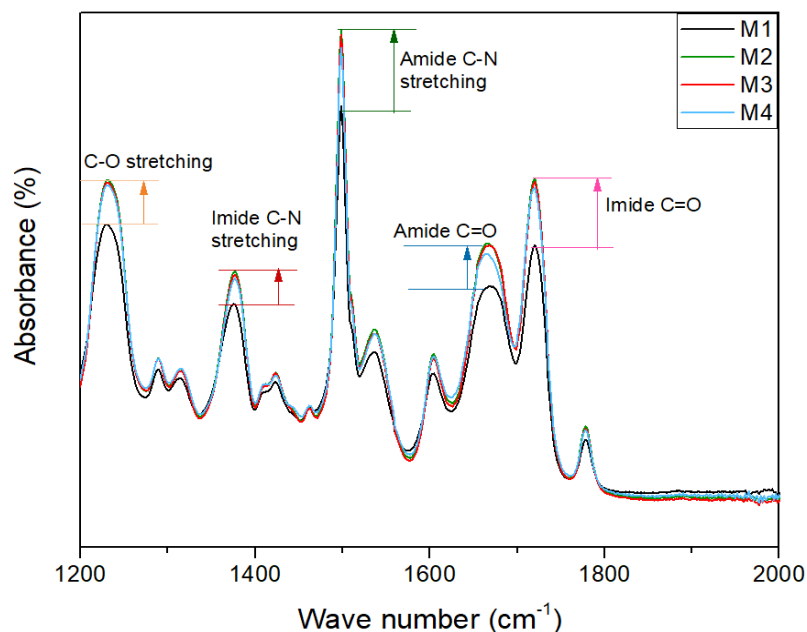


Figure 3. 5. ATR-FTIR spectra of all the membranes for scanning range 1200–2000 cm^{-1} .

3.4.4 Surface wettability:

Fig. 3.6 represents the water contact angle (WCA) of the bare PAI and bilayer coated PAI membranes. Since the underlying PAI support was identical for all membranes, the substantial change in the WCA can be attributed to the alteration of surface topography and the physicochemical properties by the deposited polyelectrolytes. The surface hydrophilicity of bilayer membranes was increased by an increase in the number of hydrophilic C–O, C=O bonds at the surface (functionality imparted by polyelectrolytes), which is evidenced by ATR-FTIR results (Fig.3.5). ATR-FTIR results clearly demonstrates an increase in the intensity of those hydrophilic functional groups, which translates into an increase in the hydrophilicity of the bilayer membrane. Hence, the WCA reduced by 12° for bilayer membranes. However, for the case of bilayer membranes (M2-M4), no significant change in the surface wettability was observed in comparison to each other, as these membranes have the same polyelectrolytes deposited on their surfaces. This result confirms the uniform deposition 1, 2, and 4 layers of polyelectrolytes on the PAI substrates, which resulted in the same WCA for membrane M2-M4. In other words, the bilayer membranes had almost the same physicochemical properties in terms of surface roughness and chemical composition, which diminished the effect of physical and chemical heterogeneities on equilibrium contact angle results.

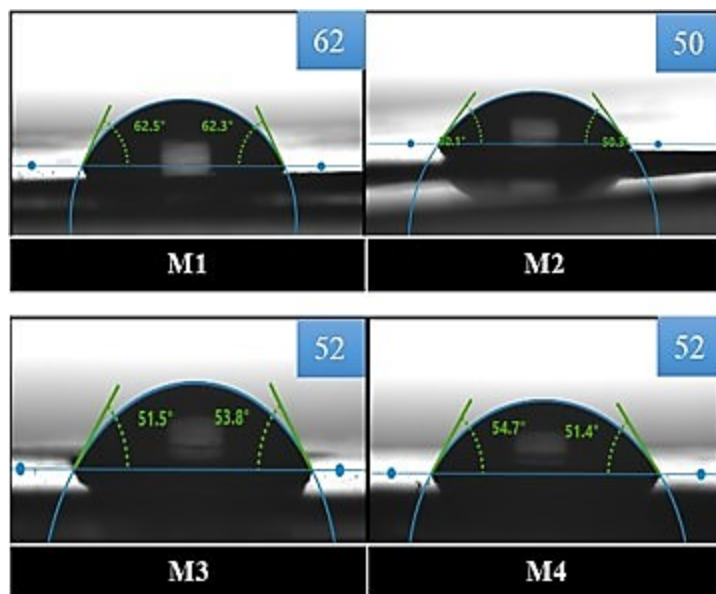


Figure 3. 6. Experimental image of water contact angle for synthesized membranes.

3.4.5 Hydraulic permeability:

Before evaluating hydraulic permeability, the membranes were compacted at 1.4 bar until a steady PWF obtained. Upon reaching steady flux, PWF was recorded at 2.75, 1.75, and 0.48 bar. The PWF values were plotted against applied pressure in Fig. 3.6 and the slope of the linear relationship between PWF and transmembrane pressure was reported as hydraulic permeability. The increase in PWF with transmembrane pressure was found to be linear for all the membranes.

As can be observed in Figure 3.7, the hydraulic permeability declined upon LbL coating. The initial PWF of membranes recorded at 2.75 bar is also presented in the inset of Fig 3.6. The initial PWF was found to decrease with increasing the number of bilayers. This suggests that the pore size of the membranes decreased due to the deposition of oppositely charged polyelectrolytes. The order of hydraulic permeability $M1 > M2 > M3 > M4$ followed the initial PWF decline accordingly.

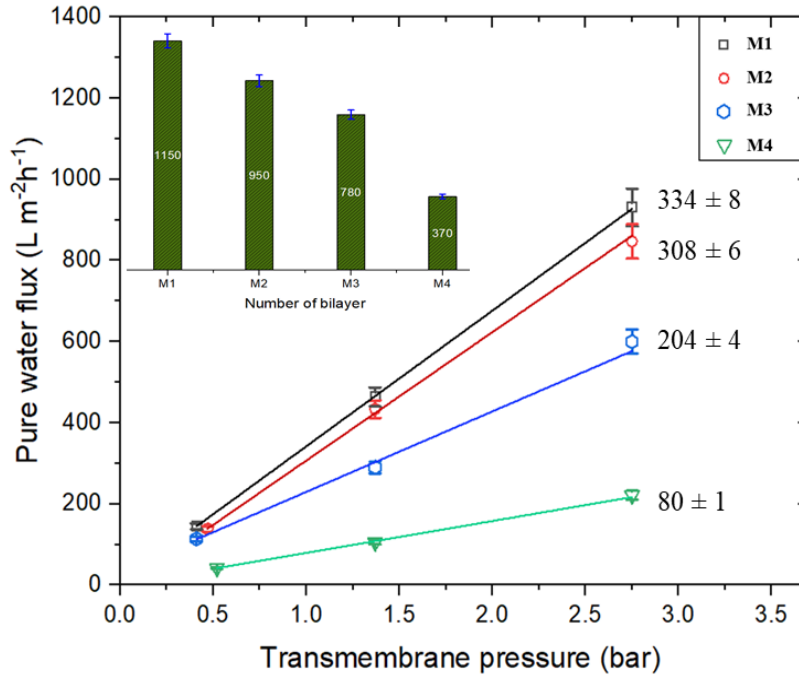


Figure 3. 7. Variation of hydraulic permeability of membrane with different number of bilayer deposition.

3.4.6 Filtration of BFW

In this section, the fouling tendency of PAI membrane was compared with PAI bilayer membranes and the permeate flux decline, organic rejection and flux recovery is reported. It is well-known fact that the fouling behavior of a membrane is influenced by several parameters including (i) hydrodynamic conditions (feed flow rate, feed channel dimensions, and permeation drag, which is related to permeation flux), (ii) feed solution chemistry (concentration of salt and organic matter, and pH), and (iii) the membrane material properties (hydrophilicity, zeta potential, and surface roughness) [127]. Hence, to explore the effectiveness of LbL assembly method in fouling reduction the first two conditions were kept constant and filtration was performed at initial permeate flux of $140 \text{ L m}^{-2} \text{ h}^{-1}$.

Fig 3.8 presents the trend of permeate flux decline of bare and bilayer PAI membranes. During BFW filtration, a rapid initial flux decline was observed initially followed by a

slower flux decline due to DOM fouling. According to the BFW component specification presented in Table 3.1, the concentration of organic matter (500 mg/L) is higher than silica

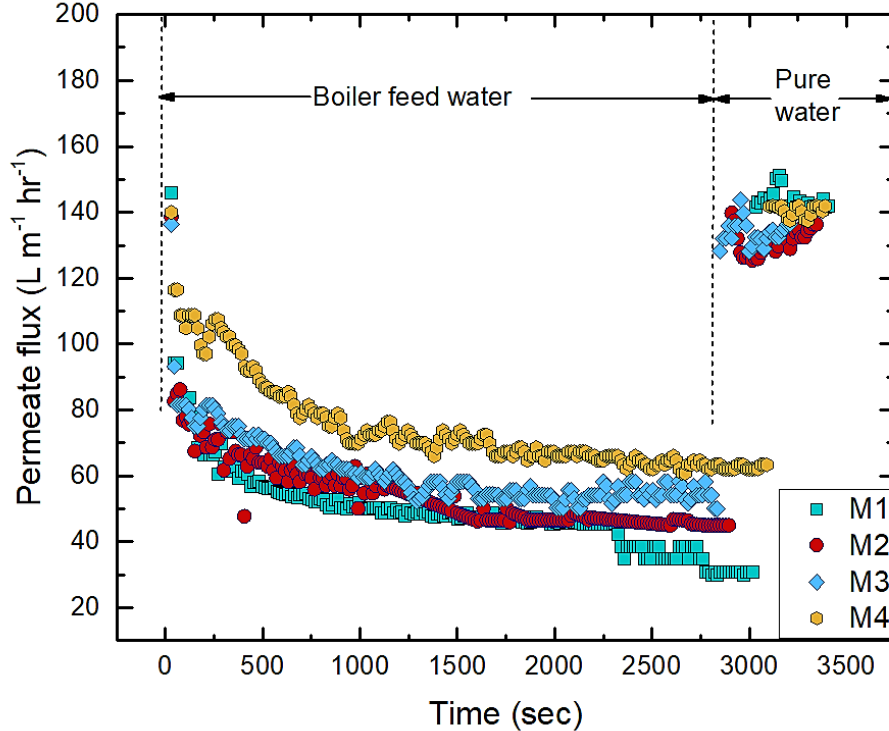


Figure 3. 8. Permeate flux decline over time due to organic fouling for all membranes.

and divalent ions concentration in the BFW (20 mg/L) and owing to small particle diameter, these divalent ions will mostly pass through a microfiltration or ultrafiltration membrane. Hence, DOM fouling is expected to be the dominant fouling mechanism in this study [107]. Organic compounds form a cake layer on the membrane surface resulting in a high resistance to permeate flow, and subsequently lowers the water flux.

The BFW mainly contains humic type organic hydrophobic acids (~40%). A more hydrophilic membrane generally repels hydrophobic foulants as enhanced hydrophilicity facilitates interaction between the membrane surface and water over interaction between membrane and hydrophobic foulants [128]. During the initial stage, gel formation over the surface and membrane pores blocking by DOM increase hydraulic resistance by inducing hydrophobic properties resulting in a sharp flux decline. However, bilayer membranes showed less initial flux decline than the pristine membrane due to their more hydrophilic

nature. In the later stage (after 100 s), flux declines in a slower rate, which can be attributed to the balance of DOM-membrane and DOM-DOM attractive forces with the hydrodynamic forces which tend to sweep the organic foulants away. For bare PAI membrane the permeate flux keeps declining in the later stages of filtration, while for bilayer membranes the permeate flux decline reaches a steady condition sooner. This result confirms the weaker DOM-membrane attraction forces in the case of bilayer membranes.

The variation of the hydrophilic/hydrophobic properties of a membrane during filtration depends on the hydrophilic/hydrophobic properties of both the membrane and the feed water constituents [128]. According to table 3.1, the BFW contains silica, divalent and monovalent salts. The presence of salts in feed significantly affect the foulant-membrane interaction. This could reduce the surface charge of membrane surface and organic macromolecules due to double layer compression and charge screening [107]. This could reduce electrostatic repulsion between membrane surface and organic foulants and elevate the deposition rate of DOM onto the membrane surface [96]. In the case of bilayer membranes, the pore walls and surface of the membrane are covered with negatively charged matter. The charge density of PAA is higher compared to PAI, which provides higher negative charge density to the membrane surface and pore walls.

Fig. 3.9(a) shows that the FD (%) reduced from 76% to 68% for one bilayer. The higher negative charge density at surface enhances the electrostatic repulsion between DOM and membrane, thus the deposition rate, i.e., permeate flux decline slows down in the case of bilayer membranes. For M3 and M4, FD (%) decreased more to 57% and 50%. A likely explanation is that the surface and the pores of the M3 and M4 membranes are more uniformly covered by the polyelectrolytes. Hence, electrostatic repulsion increased between DOM and membrane as compared to M2. Another possible reason is the smaller pore size of M3 and M4 membranes, which might have diminished the membrane pore blocking as compared to M1 and M2 membranes. The surface charge density of unmodified M1 membrane is smaller compared to bilayer membranes. Thus, organic macromolecules experience less electrostatic repulsion which leads to the formation of a closely packed thicker fouling layer. The resulting fouling layer creates comparatively higher hydraulic resistance to permeation; resulting in a high FD.

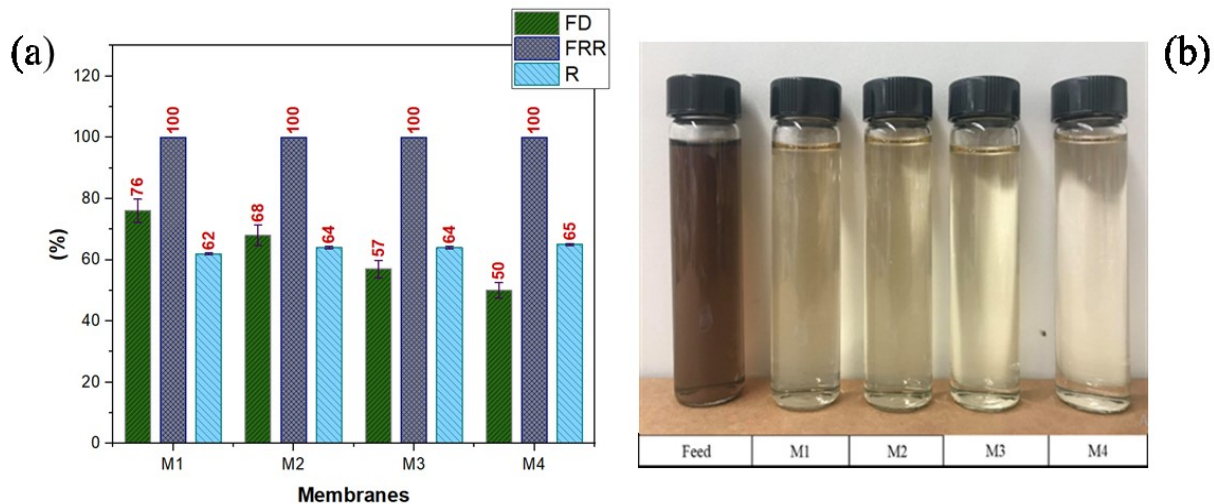


Figure 3. 9. (a) Flux decline (FD), organic matter rejection (R) and flux recovery ratio (FRR) of membranes, taken averaged over three samples. In all the cases 100% water flux recovery and almost same rejection performance was observed and (b) Image of BFW and permeate of all membranes.

All synthesized membranes showed 100% FRR, suggesting their excellent antifouling property. Fig 3.9(b) presents the image of feed and permeate. M1 had the lowest rejection of organic material (62%) due to its loose structure. For the bilayer membranes the rejection increased by 2-3%, which can be attributed to the reduced pore size by LBL coating of polyelectrolytes.

3.5 Conclusion

The PAI membrane was successfully modified by the LbL assembly approach using a polyanion (PAA) and a polycation (PDADMAC). Successful deposition was evident through numerous characterization results. The top PAA layer was always found to be negative as demonstrated by zeta potential measurement for all the bilayer membranes. The presence of PAA on the surface provided high negative charges density and higher hydrophilicity which contributed to the improvement of antifouling performance during BFW filtration. The surface negative charge density increased on the surface compared to unmodified PAI membranes, which reduced permeate flux decline by increasing electrostatic repulsion between organic matter and membrane.

Chapter 4: Conclusion and future work

4.1 Conclusion

The development of PAI MF membranes by NIPS method has opened up a new pathway for developing superhydrophilic and under water superoleophobic membranes. The inherent hydrophilic properties of PAI membranes make it a superior candidate over conventional PES and PSF MF/UF membranes. For further improving the hydrophilic property and final membrane property both blending and coating approaches were applied.

In the first part of the study, the membrane was further modified with hydrophilic additives PEG (0.4, 6 kDa) and PVP (10 kDa, 360kDa) by doping these additives into polymer solution in order to improve the oleophobicity further. The main objective in this part was to (i) fundamentally understand the role of incorporating additives in resultant membrane morphology, (ii) to identify the effect of additives in the physiochemical characteristics, (iii) to understand the combined effect of membrane morphology and physical and chemical characteristics during oil emulsion filtration performance. Upon addition of these additives the viscosity of polymer solution increase which increased the kinetic hindrance of polymer solution. The kinetic hindrance decelerated the exchange rate between solvent and non-solvent which resulted in a denser membrane matrix. The effect of adding these hydrophilic additives was systematically studied in terms of the effect on membrane porosity, permeability, under water oleophobicity, selectivity and anti-oil fouling performance. A decline in hydraulic permeability was observed for the modified membranes which was attributed to formation of relatively denser membrane. An improvement in underwater oleophobicity was observed for optimized membranes as demonstrated by underwater oil contact angle. Moreover, the use of additive enabled reducing the surface roughness as demonstrated by AFM roughness study. An improvement in permeate rate decline was observed during oil emulsion filtration for the optimized membranes, which was attributed to the advantage of having smaller pore size, smoother surface and improvement in underwater oleophobic property. These membranes were also assessed for the reusability in oil emulsion filtration. However, all the membranes exhibited almost 98% pure water regeneration capability which demonstrates the inherent

low adhesion and self-cleaning property against oil. The pure water recovery was found to be consistent in cyclic test for optimized membranes, where it kept declining for pure PAI membranes. This suggests the resultant membrane properties were further improved due to modification. The membrane exhibited excellent oil removal efficiency (98%) at a permeation rate as high as 210 ($\text{Lm}^{-2}\text{h}^{-1}$) when a very low transmembrane pressure was applied. Thus, novel PAI MF membranes demonstrated the development of highly selective, highly permeable, superhydrophilic and underwater oleophobic, energy- and cost-efficient next generation membranes for oily wastewater treatment.

In the second part of the study, the antifouling property of superhydrophilic PAI membrane against organic foulants was investigated using SAGD produced water. PAI membrane were modified by a simple and versatile LbL assembly approach using PDADMAC and PAA as oppositely charged electrolytes. The density of reactive function groups existing on a substrate play a significant part in effective deposition of oppositely charged polyelectrolyte as well as manipulates the deposition rate on the substrate. The presence of abundant reactive functional group (C-O, C=O) in the structure serves PAI membranes for being as a substrate for successful deposition of coating material for developing NF membranes. The main objective in this part was to (i) successful deposition of polyelectrolytes by LbL assembly (ii) to identify the effect of polyelectrolyte deposition on the physiochemical characteristics, (iii) to assess effect of coating on the antifouling performance of membrane during BFW filtration.

The reactive functional groups on the membrane was found to aid a very fast deposition of PDADMAC as the required time for successful deposition was as low as five minutes. The positive value of zeta potential in all pH range for membrane with one deposited layer of PDADMAC confirmed the success deposition of PDADMAC. Afterwards the negative value of zeta potential in all pH range for alternative deposited layer of PDADMAC and PAA confirmed the successful formation of bilayer on PAI substrate. The number of bilayers were increased to two and four bilayers. The change in physiochemical characteristics conducted using ATR-FTIR and EDX elemental analysis demonstrated the increase in intensity of hydrophilic groups on the membrane. The surface and pores of the membranes narrowed down due to deposition of polyelectrolytes which was evident by

decline in hydraulic permeability. The organic rejection was 62% for unmodified PAI membrane which improved up to 65% for four bilayers. The narrowing of pores due to deposited polyelectrolytes yielded increase in organic rejection. The rate of permeate decline was also improved from 76% up to 50% for four bilayers. Those improvements were attributed to presence of high density of hydrophilic functional groups on the surface and pore walls. These hydrophilic functional groups enhanced the electrostatic repulsion between organic particle and membrane surface. Increase in electrostatic repulsion helped reduce the thickness of deposited layers on the surface of membrane which ultimately resulted in lower hydraulic resistance, thus showed improvement in permeate rate decline. All the membranes showed 100% pure water recovery which demonstrated excellent antifouling property of PAI membranes towards organic foulants. However, a trace amount of rejected solutes were detected on the surface of membranes in EDX elemental analysis. A wide range of elements were detected on the surface of unmodified PAI membrane, a lot of which were not found on the surface of bilayer coated membrane. On the surface of four bilayers minimal elements were detected. During BFW filtration, enhanced negative charge on the surface prevented deposition of materials due to enhanced electrostatic repulsion between membrane surface and foulant. The washing efficiency of four bilayer membrane was supposed to enhance. The higher negative charge density on the surface resulted in enhanced interaction with water during washing step which swiped off most of the elements from the surface.

4.2 Future work

- 1) In chapter 2, the experimental results of incorporating hydrophilic additives PVP and PEG on the host membrane was presented. As a continuation of this work the performance of these membranes is worth checking in a crossflow filtration set up for oil/water emulsion filtration to compare the results obtained from dead end filtration set up. Regarding membrane modification, further studies can be done, (i) optimize the loading and the molecular weight of any additive into membrane for further improving underwater oleophobicity without deteriorating the pore size distribution permeability, selectivity and mechanical stability (ii) Explore the incorporation of different hydrophilic additives other than PVP and PEG on to the host membrane to investigate

the variation in underwater oleophobic property, surface heterogeneity and anti-oil fouling performance.

- 2) In chapter 3, the results of membranes modified by LbL assembly up to four bilayers was presented. As a continuation of this study, the number of bilayers can be increased further to investigate the organic rejection and anti-fouling performance of BFW. Regarding improving the surface functionalization, further studies can be done, (i) execute LbL deposition using higher ratio of polyelectrolyte concentration, (ii) elevate the deposition time of polyelectrolytes, (iii) execute deposition on different pH of polyelectrolyte solution to investigate the effect of variation in selectivity, permeability, surface physiochemical properties during BFW filtration.
- 3) In chapter 3, the substrate chosen for LbL deposition had MWCO around 750 kDa. As the surface is the first contact point between membrane and foulant, the surface physiochemical characteristics controls the deposition of fouling layer on the surface. The retention of solutes is still governed by the pore size of the membrane. Thus, LbL assembly conducted in chapter 3 must be conducted on a tighter substrate to evaluate the rejection performance of organic matters contained in BFW.

References

- [1] G.R. Xu, S.H. Wang, H.L. Zhao, S.B. Wu, J.M. Xu, L. Li, X.Y. Liu, Layer-by-layer (LBL) assembly technology as promising strategy for tailoring pressure-driven desalination membranes, *J. Memb. Sci.* 493 (2015) 428–443. doi:10.1016/j.memsci.2015.06.038.
- [2] R.M. Horner, C.B. Harto, R.B. Jackson, E.R. Lowry, A.R. Brandt, T.W. Yeskoo, D.J. Murphy, C.E. Clark, Water Use and Management in the Bakken Shale Oil Play in North Dakota, *Environ. Sci. Technol.* 50 (2016) 3275–3282. doi:10.1021/acs.est.5b04079.
- [3] D.M. Rockwood, Water and energy, *GeoJournal.* 3 (1979) 461–470. doi:10.1007/BF00455985.
- [4] A. Fakhru'l-Razi, A. Pendashteh, L.C. Abdullah, D.R.A. Biak, S.S. Madaeni, Z.Z. Abidin, Review of technologies for oil and gas produced water treatment, *J. Hazard. Mater.* 170 (2009) 530–551. doi:10.1016/j.jhazmat.2009.05.044.
- [5] N.A. Ochoa, M. Masuelli, J. Marchese, Effect of hydrophilicity on fouling of an emulsified oil wastewater with PVDF/PMMA membranes, *J. Memb. Sci.* 226 (2003) 203–211. doi:10.1016/j.memsci.2003.09.004.
- [6] R. Hill, Thermal In Situ Water Conservation Study A Summary Report, (2012) 1–22. <http://www.ai-ees.ca/media/6868/thermal-in-situ-water-summary-report.pdf>.
- [7] W.L. Ellsworth, Injection-Induced Earthquakes, 341 (2013) 1–8.
- [8] A. McGarr, B. Bekins, N. Burkardt, J. Dewey, P. Earle, W. Ellsworth, S. Ge, S. Hickman, A. Holland, E. Majer, J. Rubinstein, A. Sheehan, Coping with earthquakes induced by fluid injection, *Science* (80-.). 347 (2015) 830–831. doi:10.1126/science.aaa0494.
- [9] W.F. Heins, Technical advancements in SAGD evaporative produced water treatment, *J. Can. Pet. Technol.* 48 (2009) 27–32.
- [10] P. Karami, B. Khorshidi, M. McGregor, J.T. Peichel, J.B.P. Soares, M. Sadrzadeh,

- Thermally stable thin film composite polymeric membranes for water treatment: A review, *J. Clean. Prod.* (2019) 119447. doi:10.1016/j.jclepro.2019.119447.
- [11] M. Cheryan, N. Rajagopalan, Membrane processing of oily streams. *Wastewater treatment and waste reduction, J. Memb. Sci.* 151 (1998) 13–28. doi:10.1016/S0376-7388(98)00190-2.
- [12] B. Road, *Novel Fouling-Reducing Coatings for Ultrafiltration , Nanofiltration , and Reverse Osmosis Membranes*, (2007).
- [13] V.C. Onishi, E.S. Fraga, J.A. Reyes-Labarta, J.A. Caballero, Desalination of shale gas wastewater: Thermal and membrane applications for zero-liquid discharge, *Emerg. Technol. Sustain. Desalin. Handb.* (2018) 399–431. doi:10.1016/B978-0-12-815818-0.00012-6.
- [14] L.F. Greenlee, D.F. Lawler, B.D. Freeman, B. Marrot, P. Moulin, Reverse osmosis desalination: Water sources, technology, and today’s challenges, *Water Res.* 43 (2009) 2317–2348. doi:10.1016/j.watres.2009.03.010.
- [15] J. Mueller, Y. Cen, R.H. Davis, Crossflow microfiltration of oily water, *J. Memb. Sci.* 129 (1997) 221–235. doi:10.1016/S0376-7388(96)00344-4.
- [16] G. dong Kang, Y. ming Cao, Development of antifouling reverse osmosis membranes for water treatment: A review, *Water Res.* 46 (2012) 584–600. doi:10.1016/j.watres.2011.11.041.
- [17] M. Mulder, *Basic Principles of Membrane Technology*, *Zeitschrift Für Phys. Chemie.* 72 (1998) 564. doi:10.1007/978-94-009-1766-8.
- [18] U. Zhanat, E. Sharipzhan, Mechanism of Gases Transfer through Polymer Membranes and Membrane Module Calculation Model to Separate Gases, *Procedia Technol.* 1 (2012) 356–361. doi:10.1016/j.protcy.2012.02.074.
- [19] B.K. Mianae, *Advanced Thin Film Composite and Nanocomposite Polyamide Membrane for Water Treatment*, University of Alberta, 2017.
- [20] X. Li, Y. Wang, X. Lu, C. Xiao, Morphology changes of polyvinylidene fluoride

- membrane under different phase separation mechanisms, *J. Memb. Sci.* 320 (2008) 477–482. doi:10.1016/j.memsci.2008.04.033.
- [21] T. Waite, A. Fane, A. Schäfer, *Nanofiltration: Principles and Applications*, J. Am. Water Works Assoc. (2005) 121–122.
- [22] A. Mansourizadeh, A. Javadi Azad, Preparation of blend polyethersulfone/cellulose acetate/polyethylene glycol asymmetric membranes for oil-water separation, *J. Polym. Res.* 21 (2014). doi:10.1007/s10965-014-0375-x.
- [23] Q.F. Alsalhy, Hollow fiber ultrafiltration membranes prepared from blends of poly(vinyl chloride) and polystyrene, *Desalination*. 294 (2012) 44–52. doi:10.1016/j.desal.2012.03.008.
- [24] W. Salim, W.W. Ho, Recent developments on nanostructured polymer-based membranes, *Curr. Opin. Chem. Eng.* 8 (2015) 76–82. doi:10.1016/j.coche.2015.03.003.
- [25] J. Yin, B. Deng, Polymer-matrix nanocomposite membranes for water treatment, *J. Memb. Sci.* 479 (2015) 256–275. doi:10.1016/j.memsci.2014.11.019.
- [26] L. Yan, Y.S. Li, C.B. Xiang, S. Xianda, Effect of nano-sized Al₂O₃-particle addition on PVDF ultrafiltration membrane performance, *J. Memb. Sci.* 276 (2006) 162–167. doi:10.1016/j.memsci.2005.09.044.
- [27] N. Ghaemi, S.S. Madaeni, P. Daraei, H. Rajabi, S. Zinadini, A. Alizadeh, R. Heydari, M. Beygzadeh, S. Ghouzivand, Polyethersulfone membrane enhanced with iron oxide nanoparticles for copper removal from water: Application of new functionalized Fe₃O₄ nanoparticles, *Chem. Eng. J.* 263 (2015) 101–112. doi:10.1016/j.cej.2014.10.103.
- [28] B. Khorshidi, J. Hajinasiri, G. Ma, S. Bhattacharjee, M. Sadrzadeh, Thermally resistant and electrically conductive PES/ITO nanocomposite membrane, *J. Memb. Sci.* 500 (2016) 151–160. doi:10.1016/j.memsci.2015.11.015.
- [29] V. Vatanpour, S.S. Madaeni, R. Moradian, S. Zinadini, B. Astinchap, Novel

- antibifouling nanofiltration polyethersulfone membrane fabricated from embedding TiO₂ coated multiwalled carbon nanotubes, *Sep. Purif. Technol.* 90 (2012) 69–82. doi:10.1016/j.seppur.2012.02.014.
- [30] Z. Wang, H. Yu, J. Xia, F. Zhang, F. Li, Y. Xia, Y. Li, Novel GO-blended PVDF ultrafiltration membranes, *Desalination*. 299 (2012) 50–54. doi:10.1016/j.desal.2012.05.015.
- [31] C. Dong, G. He, H. Li, R. Zhao, Y. Han, Y. Deng, Antifouling enhancement of poly(vinylidene fluoride) microfiltration membrane by adding Mg(OH)₂ nanoparticles, *J. Memb. Sci.* 387–388 (2012) 40–47. doi:10.1016/j.memsci.2011.10.007.
- [32] M. Ulbricht, Advanced functional polymer membranes, *Polymer (Guildf)*. 47 (2006) 2217–2262. doi:10.1016/j.polymer.2006.01.084.
- [33] M. Padaki, A.M. Isloor, G. Belavadi, K.N. Prabhu, Preparation, characterization and performance study of poly(isobutylene- alt-maleic anhydride) [PIAM] and polysulfone [PSf] composite membranes before and after alkali treatment, *Ind. Eng. Chem. Res.* 50 (2011) 6528–6534. doi:10.1021/ie102387n.
- [34] R. Malaisamy, M.L. Bruening, High-flux nanofiltration membranes prepared by adsorption of multilayer polyelectrolyte membranes on polymeric supports, *Langmuir*. 21 (2005) 10587–10592. doi:10.1021/la051669s.
- [35] U.K. Aravind, J. Mathew, C.T. Aravindakumar, Transport studies of BSA, lysozyme and ovalbumin through chitosan/polystyrene sulfonate multilayer membrane, *J. Memb. Sci.* 299 (2007) 146–155. doi:10.1016/j.memsci.2007.04.036.
- [36] J.M. Abu Mohammad, H. Sheardown, A. Al-ahmed, eds., *Functional Polymers*, Springer, Switzerland, 2019.
- [37] P.-C. Chen, Z.-K. Xu, Mineral-Coated Polymer Membranes with Superhydrophilicity and Underwater Superoleophobicity for Effective Oil/Water Separation, *Sci. Rep.* 3 (2013) 2776. doi:10.1038/srep02776.

- [38] A.K. Kota, G. Kwon, W. Choi, J.M. Mabry, A. Tuteja, Hygro-responsive membranes for effective oil–water separation, *Nat. Commun.* 3 (2012). doi:10.1038/ncomms2027.
- [39] H.H. Sokker, N.M. El-Sawy, M.A. Hassan, B.E. El-Anadouli, Adsorption of crude oil from aqueous solution by hydrogel of chitosan based polyacrylamide prepared by radiation induced graft polymerization, *J. Hazard. Mater.* 190 (2011) 359–365. doi:10.1016/j.jhazmat.2011.03.055.
- [40] G. Deschamps, H. Caruel, M.-E. Borredon, C. Bonnin, C. Vignoles, Oil Removal from Water by Selective Sorption on Hydrophobic Cotton Fibers. 1. Study of Sorption Properties and Comparison with Other Cotton Fiber-Based Sorbents, *Environ. Sci. Technol.* 37 (2003) 1013–1015. doi:10.1021/es020061s.
- [41] I. Aranberri, B.P. Binks, J.H. Clint, P.D.I. Fletcher, Evaporation Rates of Water from Concentrated Oil-in-Water Emulsions, *Langmuir.* 20 (2004) 2069–2074. doi:10.1021/la035031x.
- [42] J. Kong, K. Li, Oil removal from oil-in-water emulsions using PVDF membranes, *Sep. Purif. Technol.* 16 (1999) 83–93. doi:10.1016/S1383-5866(98)00114-2.
- [43] L. Ben Mansour, S. Chalbi, Removal of oil from oil/water emulsions using electroflotation process, *J. Appl. Electrochem.* 36 (2006) 577–581. doi:10.1007/s10800-005-9109-4.
- [44] M.H. Alhaji, K. Sanaullah, S.-F. Lim, A. Khan, C.N. Hipolito, M.O. Abdullah, S.A. Bhawani, T. Jamil, Photocatalytic treatment technology for palm oil mill effluent (POME) – A review, *Process Saf. Environ. Prot.* 102 (2016) 673–686. doi:10.1016/j.psep.2016.05.020.
- [45] I.-S. Chang, C.-M. Chung, S.-H. Han, Treatment of oily wastewater by ultrafiltration and ozone, *Desalination.* 133 (2001) 225–232. doi:10.1016/S0011-9164(01)00103-5.
- [46] S. Munirasu, M.A. Haija, F. Banat, Use of membrane technology for oil field and refinery produced water treatment—A review, *Process Saf. Environ. Prot.* 100

- (2016) 183–202. doi:10.1016/J.PSEP.2016.01.010.
- [47] S. Wang, Y. Song, L. Jiang, Microscale and nanoscale hierarchical structured mesh films with superhydrophobic and superoleophilic properties induced by long-chain fatty acids, *Nanotechnology*. 18 (2006) 015103. doi:10.1088/0957-4484/18/1/015103.
- [48] C.H. Lee, N. Johnson, J. Drelich, Y.K. Yap, The performance of superhydrophobic and superoleophilic carbon nanotube meshes in water–oil filtration, *Carbon N. Y.* 49 (2011) 669–676. doi:http://dx.doi.org/10.1016/j.carbon.2010.10.016.
- [49] D.-D. La, T.A. Nguyen, S. Lee, J.W. Kim, Y.S. Kim, A stable superhydrophobic and superoleophilic Cu mesh based on copper hydroxide nanoneedle arrays, *Appl. Surf. Sci.* 257 (2011) 5705–5710. doi:10.1016/j.apsusc.2011.01.078.
- [50] M. Liu, S. Wang, Z. Wei, Y. Song, L. Jiang, Bioinspired design of a superoleophobic and low adhesive water/solid interface, *Adv. Mater.* 21 (2009) 665–669. doi:10.1002/adma.200801782.
- [51] P.R. Waghmare, N.S.K. Gunda, S.K. Mitra, Under-water superoleophobicity of fish scales., *Sci. Rep.* 4 (2014) 7454. doi:10.1038/srep07454.
- [52] D. Tian, X. Zhang, X. Wang, J. Zhai, L. Jiang, Micro/nanoscale hierarchical structured ZnO mesh film for separation of water and oil, *Phys. Chem. Chem. Phys.* 13 (2011) 14606. doi:10.1039/c1cp20671k.
- [53] Y.C. Jung, B. Bhushan, Wetting Behavior of Water and Oil Droplets in Three-Phase Interfaces for Hydrophobicity/philicity and Oleophobicity/philicity †, *Langmuir*. 25 (2009) 14165–14173. doi:10.1021/la901906h.
- [54] M. Sadrzadeh, E. Gorouhi, T. Mohammadi, Oily wastewater treatment using polytetrafluoroethylene (PTFE) hydrophobic membranes, in: *Twelfth Int. Water Technol. Conf.*, Alexandria, Egypt, 2008: pp. 783–793.
- [55] E. Gorouhi, M. Sadrzadeh, T. Mohammadi, Microfiltration of oily wastewater using PP hydrophobic membrane, *Desalination*. 200 (2006) 319–321.

- [56] K. Liu, X. Yao, L. Jiang, Recent developments in bio-inspired special wettability, *Chem. Soc. Rev.* 39 (2010) 3240–3255.
- [57] J. Ju, T. Wang, Q. Wang, Superhydrophilic and underwater superoleophobic PVDF membranes via plasma-induced surface PEGDA for effective separation of oil-in-water emulsions, *Colloids Surfaces A Physicochem. Eng. Asp.* 481 (2015) 151–157. doi:10.1016/j.colsurfa.2015.01.041.
- [58] Q. Liu, A.A. Patel, L. Liu, Superhydrophilic and Underwater Superoleophobic Poly(sulfobetaine methacrylate)-Grafted Glass Fiber Filters for Oil–Water Separation, *ACS Appl. Mater. Interfaces.* 6 (2014) 8996–9003. doi:10.1021/am502302g.
- [59] G. Zhang, X. Zhang, Y. Huang, Z. Su, A surface exhibiting superoleophobicity both in air and in seawater, *ACS Appl. Mater. Interfaces.* 5 (2013) 6400–6403. doi:10.1021/am401582d.
- [60] H. Bai, X. Wang, Y. Zhou, L. Zhang, Preparation and characterization of poly(vinylidene fluoride) composite membranes blended with nano-crystalline cellulose, *Prog. Nat. Sci. Mater. Int.* 22 (2012) 250–257. doi:10.1016/j.pnsc.2012.04.011.
- [61] Z. Xue, S. Wang, L. Lin, L. Chen, M. Liu, L. Feng, L. Jiang, A novel superhydrophilic and underwater superoleophobic hydrogel-coated mesh for oil/water separation, *Adv. Mater.* 23 (2011) 4270–4273.
- [62] A. Kusumaatmaja, N. Fauji, K. Triyana, Polysulfone/Polyacrylonitrile Membrane for Oil/Water Separation, *Mater. Sci. Forum.* 886 (2017) 145–149. doi:10.4028/www.scientific.net/MSF.886.145.
- [63] M. Obaid, N.A.M. Barakat, O.A. Fadali, M. Motlak, A.A. Almajid, K.A. Khalil, Effective and reusable oil/water separation membranes based on modified polysulfone electrospun nanofiber mats, *Chem. Eng. J.* 259 (2015) 449–456. doi:10.1016/j.cej.2014.07.095.
- [64] A. Pagidi, R. Saranya, G. Arthanareeswaran, A.F. Ismail, T. Matsuura, Enhanced

- oil-water separation using polysulfone membranes modified with polymeric additives, *Desalination*. 344 (2014) 280–288. doi:10.1016/j.desal.2014.03.033.
- [65] Y. Wang, S.H. Goh, T.S. Chung, Miscibility study of Torlon®polyamide-imide with Matrimid®5218 polyimide and polybenzimidazole, *Polymer (Guildf)*. 48 (2007) 2901–2909. doi:10.1016/j.polymer.2007.03.040.
- [66] C.J. Van Oss, *Interfacial forces in aqueous media*, CRC press, 2006.
- [67] J.A. Brant, A.E. Childress, Assessing short-range membrane – colloid interactions using surface energetics, 203 (2002) 257–273.
- [68] M. Rastgar, A. Shakeri, A. Bozorg, H. Salehi, V. Saadattalab, Highly-efficient forward osmosis membrane tailored by magnetically responsive graphene oxide/Fe₃O₄nanohybrid, *Appl. Surf. Sci.* 441 (2018) 923–935. doi:10.1016/j.apsusc.2018.02.118.
- [69] A. Maiti, M. Sadrzadeh, S. Guha Thakurta, D.J. Pernitsky, S. Bhattacharjee, Characterization of boiler blowdown water from steam-assisted gravity drainage and silica–organic coprecipitation during acidification and ultrafiltration, *Energy & Fuels*. 26 (2012) 5604–5612. doi:10.1021/ef300865e.
- [70] R. Wang, L. Shi, C.Y. Tang, S. Chou, C. Qiu, A.G. Fane, Characterization of novel forward osmosis hollow fiber membranes, *J. Memb. Sci.* 355 (2010) 158–167. doi:10.1016/j.memsci.2010.03.017.
- [71] M. Rastgar, A. Bozorg, A. Shakeri, Novel Dimensionally Controlled Nanopore Forming Template in Forward Osmosis Membranes, *Environ. Sci. Technol.* 52 (2018) 2704–2716. doi:10.1021/acs.est.7b05583.
- [72] M. Sadrzadeh, S. Bhattacharjee, Rational design of phase inversion membranes by tailoring thermodynamics and kinetics of casting solution using polymer additives, *J. Memb. Sci.* 441 (2013) 31–44. doi:10.1016/j.memsci.2013.04.009.
- [73] R. Rohani, M. Hyland, D. Patterson, A refined one-filtration method for aqueous based nanofiltration and ultrafiltration membrane molecular weight cut-off

- determination using polyethylene glycols, *J. Memb. Sci.* 382 (2011) 278–290.
doi:10.1016/j.memsci.2011.08.023.
- [74] J.I. Calvo, R.I. Peinador, P. Prádanos, L. Palacio, A. Bottino, G. Capannelli, A. Hernández, Liquid-liquid displacement porosimetry to estimate the molecular weight cut-off of ultrafiltration membranes, *Desalination*. 268 (2011) 174–181.
doi:10.1016/j.desal.2010.10.016.
- [75] P. Aimar, M. Meireles, V. Sanchez, A contribution to the translation of retention curves into pore size distributions for sieving membranes, *J. Memb. Sci.* 54 (1990) 321–338. doi:10.1016/S0376-7388(00)80618-3.
- [76] T. He, M. Frank, M.H.V. Mulder, M. Wessling, Preparation and characterization of nanofiltration membranes by coating polyethersulfone hollow fibers with sulfonated poly(ether ether ketone) (SPEEK), *J. Memb. Sci.* 307 (2008) 62–72.
doi:10.1016/j.memsci.2007.09.016.
- [77] L. Yu, Y. Zhang, B. Zhang, J. Liu, H. Zhang, C. Song, Preparation and characterization of HPEI-GO / PES ultra filtration membrane with antifouling and antibacterial properties, *J. Memb. Sci.* 447 (2013) 452–462.
doi:10.1016/j.memsci.2013.07.042.
- [78] Y. Zhang, R. Wang, L. Zhang, A.G. Fane, Novel single-step hydrophobic modification of polymeric hollow fiber membranes containing imide groups : Its potential for membrane contactor application, *Sep. Purif. Technol.* 101 (2012) 76–84. doi:10.1016/j.seppur.2012.09.009.
- [79] A. Karkooti, A.Z. Yazdi, P. Chen, M. McGregor, N. Nazemifard, M. Sadrzadeh, Development of advanced nanocomposite membranes using graphene nanoribbons and nanosheets for water treatment, *J. Memb. Sci.* 560 (2018) 97–107.
doi:10.1016/j.memsci.2018.04.034.
- [80] P.J. Larkin, *IR and Raman Spectra–Structure Correlations*, 2018.
doi:10.1016/B978-0-12-804162-8.00006-9.
- [81] M. Amirilargani, M. Sadrzadeh, T. Mohammadi, Synthesis and characterization of

polyethersulfone membranes, *J. Polym. Res.* 17 (2010) 363–377.
doi:10.1007/s10965-009-9323-6.

- [82] E. Saljoughi, M. Sadrzadeh, T. Mohammadi, Effect of preparation variables on morphology and pure water permeation flux through asymmetric cellulose acetate membranes, *J. Memb. Sci.* 326 (2009) 627–634.
doi:10.1016/j.memsci.2008.10.044.
- [83] I.M. Wienk, R.M. Boom, M.A.M. Beerlage, A.M.W. Bulte, C.A. Smolders, H. Strathmann, Recent advances in the formation of phase inversion membranes made from amorphous or semi-crystalline polymers, 113 (1996) 361–371.
- [84] H. Strathmann, K. Kock, The formation mechanism of phase inversion membranes, *Desalination*. 21 (1977) 241–255. doi:10.1016/S0011-9164(00)88244-2.
- [85] E. Saljoughi, M. Amirilargani, T. Mohammadi, Effect of Poly (vinyl pyrrolidone) Concentration and Coagulation Bath Temperature on the Morphology , Permeability , and Thermal Stability of Asymmetric Cellulose Acetate Membranes, *J. Appl. Polym. Sci.* 111 (2008) 2537–2544. doi:10.1002/app.
- [86] J. Kim, K. Lee, Effect of PEG additive on membrane formation by phase inversion_1998.pdf, 138 (1998) 153–163.
- [87] C.A. Smolders, A.J. Reuvers, R.M. Boom, I.M. Wienk, Microstructures in phase-inversion membranes. Part 1. Formation of macrovoids, *J. Memb. Sci.* 73 (1992) 259–275. doi:10.1016/0376-7388(92)80134-6.
- [88] Remko Boom, By immersion, *Membr. Form. BY Immers. Precip. ROLE A Polym. Addit.* (1965) 3–240.
- [89] C. Jan, V. Oss, Development and applications of the interfacial tension between water and organic or biological surfaces, 54 (2007) 2–9.
doi:10.1016/j.colsurfb.2006.05.024.
- [90] R.N. Wenzel, Resistance of solid surfaces to wetting by water, *Ind. Eng. Chem.* 28

- (1936) 988–994. doi:10.1021/ie50320a024.
- [91] G. Hurwitz, G.R. Guillen, E.M. V Hoek, Probing polyamide membrane surface charge , zeta potential , wettability , and hydrophilicity with contact angle measurements, *J. OfMembrane Sci.* 349 (2010) 349–357.
doi:10.1016/j.memsci.2009.11.063.
- [92] B. Khorshidi, B. Soltannia, T. Thundat, M. Sadrzadeh, Synthesis of thin film composite polyamide membranes: Effect of monohydric and polyhydric alcohol additives in aqueous solution, *J. Membr. Sci. J.* 523 (2017) 336–345.
doi:10.1016/j.memsci.2016.09.062.
- [93] B. Khorshidi, T. Thundat, D. Pernitsky, M. Sadrzadeh, A parametric study on the synergistic impacts of chemical additives on permeation properties of thin film composite polyamide membrane, *J. Memb. Sci.* 535 (2017) 248–257.
doi:10.1016/j.memsci.2017.04.052.
- [94] N. Subhi, A.R.D. Verliefde, V. Chen, P. Le-clech, Assessment of physicochemical interactions in hollow fibre ultrafiltration membrane by contact angle analysis, *J. Memb. Sci.* 403–404 (2012) 32–40. doi:10.1016/j.memsci.2012.02.007.
- [95] A.S. Jönsson, B. Jönsson, Ultrafiltration of colloidal dispersions - A theoretical model of the concentration polarization phenomena, *J. Colloid Interface Sci.* 180 (1996) 504–518. doi:10.1006/jcis.1996.0331.
- [96] S. Hong, M. Elimelech, Chemical and physical aspects of natural organic matter (NOM) fouling of nanofiltration membranes, *J. Memb. Sci.* 132 (1997) 159–181.
doi:10.1016/S0376-7388(97)00060-4.
- [97] K. Liu, Y. Tian, L. Jiang, Bio-inspired superoleophobic and smart materials: Design, fabrication, and application, *Prog. Mater. Sci.* 58 (2013) 503–564.
doi:10.1016/j.pmatsci.2012.11.001.
- [98] X. Tian, V. Jokinen, J. Li, J. Sainio, R.H.A. Ras, Unusual Dual Superlyophobic Surfaces in Oil – Water Systems : The Design Principles, *Adv. Mater.* (2016) 10652–10658. doi:10.1002/adma.201602714.

- [99] Y. Huang, H. Li, L. Wang, Y. Qiao, C. Tang, C. Jung, Y. Yoon, Ultrafiltration Membranes with Structure-Optimized Graphene-Oxide Coatings for Antifouling Oil / Water Separation, *Adv. Mater. Interfaces.* (2015) 1–7. doi:10.1002/admi.201400433.
- [100] X. Deng, L. Mammen, H.-J. Butt, D. Vollmer, Supporting Online Material for: Candle Soot as a Template for a Transparent Robust Superamphiphobic Coating, *Science* (80-.). 335 (2012) 1–12. doi:10.1126/science.1207115.
- [101] B. Chakrabarty, A.K. Ghoshal, M.K. Purkait, Ultrafiltration of stable oil-in-water emulsion by polysulfone membrane, *J. Memb. Sci.* 325 (2008) 427–437. doi:10.1016/j.memsci.2008.08.007.
- [102] Q. Ma, H. Cheng, A.G. Fane, R. Wang, H. Zhang, Recent Development of Advanced Materials with Special Wettability for Selective Oil/Water Separation, *Small.* 12 (2016) 2186–2202. doi:10.1002/smll.201503685.
- [103] L. Feng, Z. Zhang, Z. Mai, Y. Ma, B. Liu, L. Jiang, D. Zhu, A super-hydrophobic and super-oleophilic coating mesh film for the separation of oil and water, *Angew. Chemie - Int. Ed.* 43 (2004) 2012–2014. doi:10.1002/anie.200353381.
- [104] Z. Shi, W. Zhang, F. Zhang, X. Liu, D. Wang, J. Jin, L. Jiang, Ultrafast separation of emulsified oil/water mixtures by ultrathin free-standing single-walled carbon nanotube network films, *Adv. Mater.* 25 (2013) 2422–2427. doi:10.1002/adma.201204873.
- [105] S. Huang, R.H.A. Ras, X. Tian, ScienceDirect Antifouling membranes for oily wastewater treatment : Interplay between wetting and membrane fouling, *Curr. Opin. Colloid Interface Sci.* 36 (2018) 90–109. doi:10.1016/j.cocis.2018.02.002.
- [106] M. Hayatbakhsh, M. Sadrzadeh, D. Pernitsky, S. Bhattacharjee, J. Hajinasiri, Treatment of an in situ oil sands produced water by polymeric membranes, *Desalin. Water Treat.* 57 (2016). doi:10.1080/19443994.2015.1069216.
- [107] M. Sadrzadeh, J. Hajinasiri, S. Bhattacharjee, D. Pernitsky, Nanofiltration of oil sands boiler feed water: Effect of pH on water flux and organic and dissolved solid

- rejection, *Sep. Purif. Technol.* 141 (2015) 339–353.
doi:10.1016/j.seppur.2014.12.011.
- [108] H. Peng, K. Volchek, M. MacKinnon, W.P. Wong, C.E. Brown, Application on to nanofiltration to water management options for oil sands operation, *Desalination*. 170 (2004) 137–150. doi:10.1016/j.desal.2004.03.018.
- [109] S.E. Hrudey, Z. Xu, Environmental and Health Impacts of Canada ' s Oil Sands Industry, *Engineering*. (2010) 22.
http://www.rsc.ca/documents/expert/RSC_Exp_ExecutiveSummary_ENG_Dec14_10_FINAL_v5.pdf.
- [110] D.W. Jennings, A. Shaikh, Heat-exchanger deposition in an inverted steam-assisted gravity drainage operation. Part 1. Inorganic and organic analyses of deposit samples, *Energy and Fuels*. 21 (2007) 176–184. doi:10.1021/ef060109d.
- [111] T. Pugsley, D.J. Pernitsky, J. Grundler, E.E. Johnsen, Fouling of Heat Transfer Surfaces in a Steam Assisted Gravity Drainage (Sagd) in Situ Facility for the Recovery of Oil Sands Bitumen, *Proc. Int. Con. Heat Exch. Fouling Clean*. 2013 (2013) 116–123.
- [112] C.A. Dyke, C.R. Bartels, Removal of organics from offshore produced waters using nanofiltration membrane technology, *Environ. Prog.* 9 (1990) 183–186. doi:10.1002/ep.670090320.
- [113] J. Diep, A. Tek, L. Thompson, J. Frommer, R. Wang, V. Piunova, J. Sly, Y.H. La, Layer-by-layer assembled core–shell star block copolymers for fouling resistant water purification membranes, *Polymer (Guildf)*. 103 (2016) 468–477. doi:10.1016/j.polymer.2015.11.048.
- [114] G. Zhang, W. Gu, S. Ji, Z. Liu, Y. Peng, Z. Wang, Preparation of polyelectrolyte multilayer membranes by dynamic layer-by-layer process for pervaporation separation of alcohol/water mixtures, *J. Memb. Sci.* 280 (2006) 727–733. doi:10.1016/j.memsci.2006.02.031.
- [115] G. Decher, J.D. Hong, J. Schmitt, Buildup of ultrathin multilayer films by a self-

assembly process: III. Consecutively alternating adsorption of anionic and cationic polyelectrolytes on charged surfaces, *Thin Solid Films*. 210–211 (1992) 831–835. doi:10.1016/0040-6090(92)90417-A.

- [116] Y. Kang, L. Emdadi, M.J. Lee, D. Liu, B. Mi, Layer-by-Layer Assembly of Zeolite/Polyelectrolyte Nanocomposite Membranes with High Zeolite Loading, *Environ. Sci. Technol. Lett.* 1 (2014) 504–509. doi:10.1021/ez500335q.
- [117] Z. Zhao, S. Shi, H. Cao, Y. Li, B. Van der Bruggen, Layer-by-layer assembly of anion exchange membrane by electrodeposition of polyelectrolytes for improved antifouling performance, *J. Memb. Sci.* 558 (2018) 1–8. doi:10.1016/j.memsci.2018.04.035.
- [118] R. Hadj Lajimi, E. Ferjani, M.S. Roudesli, A. Deratani, Effect of LbL surface modification on characteristics and performances of cellulose acetate nanofiltration membranes, *Desalination*. 266 (2011) 78–86. doi:10.1016/j.desal.2010.08.005.
- [119] W. Jin, A. Toutianoush, B. Tieke, Size- and charge-selective transport of aromatic compounds across polyelectrolyte multilayer membranes, *Appl. Surf. Sci.* 246 (2005) 444–450. doi:10.1016/j.apsusc.2004.11.067.
- [120] F. Diagne, R. Malaisamy, V. Boddie, R.D. Holbrook, B. Eribo, K.L. Jones, Polyelectrolyte and silver nanoparticle modification of microfiltration membranes to mitigate organic and bacterial fouling, *Environ. Sci. Technol.* 46 (2012) 4025–4033. doi:10.1021/es203945v.
- [121] L. Yong, A. Wahab, C. Yin, A review on nanofiltration membrane fabrication and modification using polyelectrolytes : Effective ways to develop membrane selective barriers and rejection capability, *Adv. Colloid Interface Sci.* 197–198 (2013) 85–107. doi:10.1016/j.cis.2013.04.004.
- [122] H. Guo, M. Chen, Q. Liu, Z. Wang, S. Cui, G. Zhang, LbL assembly of sulfonated cyclohexanone – formaldehyde condensation polymer and poly (ethyleneimine) towards rejection of both cationic ions and dyes, *Desalination*. 365 (2015) 108–116. doi:10.1016/j.desal.2015.01.021.

- [123] L. Yong, A. Wahab, C. Yin, C. Peng, R. Rohani, Development of nanofiltration membrane with high salt selectivity and performance stability using polyelectrolyte multilayers, *Desalination*. 351 (2014) 19–26.
doi:10.1016/j.desal.2014.07.020.
- [124] L. Wang, N. Wang, J. Li, J. Li, W. Bian, S. Ji, Layer-by-layer self-assembly of polycation/GO nanofiltration membrane with enhanced stability and fouling resistance, *Sep. Purif. Technol.* 160 (2016) 123–131.
doi:10.1016/j.seppur.2016.01.024.
- [125] A.E. Childress, M. Elimelech, Effect of solution chemistry on the surface charge of polymeric reverse osmosis and nanofiltration membranes, *J. Memb. Sci.* 119 (1996) 253–268. doi:10.1016/0376-7388(96)00127-5.
- [126] A. Karkooti, A.Z. Yazdi, P. Chen, M. Mcgregor, N. Nazemifard, Author ' s Accepted Manuscript, *J. Memb. Sci.* (2018). doi:10.1016/j.memsci.2018.04.034.
- [127] B. Khorshidi, B. Soltannia, T. Thundat, M. Sadrzadeh, crossmark, *J. Membr. Sci.* J. 523 (2017) 336–345. doi:10.1016/j.memsci.2016.09.062.
- [128] K.L. Tu, A.R. Chivas, L.D. Nghiem, Effects of membrane fouling and scaling on boron rejection by nanofiltration and reverse osmosis membranes, *Desalination*. 279 (2011) 269–277. doi:10.1016/j.desal.2011.06.019.